



1 Simulating organic aerosol in Delhi with WRF-Chem using the VBS 2 approach: Exploring model uncertainty with a Gaussian Process 3 emulator

4 Ernesto Reyes-Villegas^{1,a}, Douglas Lowe^{1,b}, Jill S. Johnson^{2,c}, Kenneth S. Carslaw², Eoghan Darbyshire^{1,d},
5 Michael Flynn¹, James D. Allan^{1,e}, Hugh Coe¹, Ying Chen³, Oliver Wild³, Scott Archer-Nicholls⁴, Alex
6 Archibald⁴, Siddhartha Singh⁵, Manish Shrivastava⁶, Rahul A. Zaveri⁶, Vikas Singh⁷, Gufran Beig⁸,
7 Ranjeet Sokhi⁹, Gordon McFiggans¹

8 ¹Department of Earth and Environmental Sciences, University of Manchester, Manchester, M13 9PL, UK

9 ²Institute for Climate and Atmospheric Science, School of Earth and Environment, University of Leeds, Leeds, LS2 9JT, UK

10 ³Lancaster Environment Centre, Lancaster University, Lancaster, LA1 4YQ, UK

11 ⁴NCAS-Climate, Department of Chemistry, University of Cambridge, Cambridge, CB2 1EW, UK

12 ⁵Ozone Unit, India Meteorology Department, New Delhi, 110003, India

13 ⁶Atmospheric Sciences & Global Change Division, Pacific Northwest National Laboratory, Richland, Washington 99352,
14 United States

15 ⁷National Atmospheric Research Laboratory, Gadanki, AP, India

16 ⁸National Institute of Advanced Studies, IISc Campus, Bengaluru, India

17 ⁹Centre for Atmospheric and Climate Physics Research, University of Hertfordshire, Hertfordshire, AL10 9AB, UK

18 ^a now at: School of Engineering and Sciences, Tecnológico de Monterrey, Guadalajara, 45201, Mexico

19 ^b now at: IT Services, University of Manchester, Manchester, M13 9PL, UK

20 ^c now at University of Sheffield, Sheffield, S10 2TN, UK

21 ^d now at: The Conflict and Environment Observatory, Hebden Bridge, HX7 5HZ, UK

22 ^e National Centre for Atmospheric Science, The University of Manchester, Manchester, M13 9PL, UK

23

24 *Correspondence to:* Gordon McFiggans (g.mcfiggans@manchester.ac.uk)

25 **Abstract.** The nature and origin of organic aerosol in the atmosphere remain unclear. The gas-particle partitioning of semi-
26 volatile organic compounds (SVOC) that constitute primary organic aerosols (POA) and the multigenerational chemical aging
27 of SVOCs are particularly poorly understood. The volatility basis set (VBS) approach, implemented in air quality models such
28 as the Weather Research and Forecasting model coupled with Chemistry (WRF-Chem), can be a useful tool to describe POA
29 production and aging. However, the main disadvantage is its complexity, making the evaluation of model uncertainty and the
30 optimal model parameterisation expensive to probe using only WRF-Chem simulations. Gaussian process emulators, trained
31 on simulations from relatively few WRF-Chem simulations, are capable of reproducing model results and estimating the
32 sources of model uncertainty within a defined range of model parameters. In this study, a WRF-Chem VBS parameterisation
33 is proposed; we then generate a perturbed parameter ensemble of 111 model runs, perturbing ten parameters of the WRF-Chem
34 model relating to organic aerosol emissions and the VBS oxidation reactions. This allowed us to cover the model's uncertainty
35 space and compare output from each run to aerosol mass spectrometer observations of organic aerosol concentrations and O:C
36 ratios measured in New Delhi, India. The simulations spanned the organic aerosol concentrations measured with the aerosol
37 mass spectrometer (AMS). However, they also highlighted potential structural errors in the model that may be related to
38 unsuitable diurnal cycles in the emissions and/or failure to adequately represent the dynamics of the planetary boundary layer.
39 While the structural errors prevented us from clearly identifying an optimised VBS approach in WRF-Chem, we were able to
40 apply the emulator in two periods: the full period (1st -29th May) and the period 14:00- 16:00 hrs local time, 1st-29th May.
41 The combination of emulator analysis and model evaluation metrics allowed us to identify plausible parameter combinations



42 for the analysed periods. We demonstrate that the methodology presented in this study can be used to determine the model
43 uncertainty and identify the appropriate parameter combination for the VBS approach, and hence provide valuable information
44 to improve our understanding on SOA production.

45 1 Introduction

46 Over the last decades, India has been facing air pollution problems and is ranked fifth in the 2020 world air quality ranking
47 (IQair, 2021) and Delhi ranked as one of the most polluted cities in the world with related health burden of about 10,000
48 premature deaths annually (Chen et al., 2020a), based on PM_{2.5} measurements (particulate matter lower than 2.5 micrometers
49 in diameter). This situation has a remarkable impact on Indian citizens due to India having a population that is larger than one
50 billion inhabitants. Organic aerosols (OA) are one of the main constituents of submicron particulate matter, accounting for
51 between 20% – 90% of the total aerosol mass concentration globally (Kanakidou et al., 2005; Zhang et al., 2007).

52 Various studies have been performed in India looking at the particulate matter composition and source identification of OA
53 using receptor modelling tools (Kompalli et al., 2020; Jain et al., 2020; Cash et al., 2021; Reyes-Villegas et al., 2021) along
54 with investigating the health risks associated with aerosols (Shivani et al., 2019; Gadi et al., 2019). However, one limitation of
55 receptor models is that they do not involve chemical processing. The use of regional atmospheric models allows the study of
56 the temporal and spatial behaviour of various chemical species of OA. The Weather Research and Forecasting model coupled
57 with Chemistry (WRF-Chem) is a regional 3-D atmospheric model that simulates the emissions and dispersion of gaseous and
58 particulate species, including the chemical processes and their interaction with meteorology. There have been recent WRF-
59 Chem studies investigating PM_{2.5} concentrations (Bran and Srivastava, 2017; Chen et al., 2020b; Jat et al., 2021) and VOC
60 compounds (Chutia et al., 2019) over India.

61 Despite the recent studies on aerosol sources and processes involving both observations and modelling, there is still a gap
62 between observations and modelling studies, for example with particulate organic matter being generally underestimated by
63 models (Bergström et al., 2012; Tsigaridis et al., 2014), mainly attributed to the lack of understanding of the emission sources
64 and the POA processes. Hence, we need to understand the capability of organic matter to produce and retain fine particulate
65 mass in order to fully understand their processes and impacts on air quality and climate (Carlton et al., 2010; von
66 Schneidmesser et al., 2015). It is here where the volatility basis set (VBS) scheme can be valuable when implemented in
67 chemical transport models. The VBS scheme describes the chemical ageing of particulate organic matter, its chemical
68 processing and associated volatility (Donahue et al., 2006; Shrivastava et al., 2011). It treats POA emissions as semi volatile
69 and distributes particulate organic matter by its volatility. This distribution, based on their saturation concentration (C*),
70 includes low volatility (LVOC), semivolatile (SVOC) and intermediate volatility (IVOC) organic compounds (Tsimpidi et al.,
71 2016). POA constitutes emissions from anthropogenic combustion processes and open biomass burning (Stewart et al., 2021a;
72 Stewart et al., 2021b) and by being considered to be semivolatile, the initial particulate organic matter partially evaporates due
73 to atmospheric dilution followed by the oxidation of evaporated semi-volatile organic vapors. The resulting low volatility
74 oxidized organic vapors can condense to produce oxidized primary organic aerosols (oPOA) (Shrivastava et al., 2008). This
75 favours the formation of IVOCs and SVOCs in the gas phase. Previous studies have found that IVOCs and SVOCs can act as
76 a reservoir of organic species that are able to repartition to the particle phase after suffering chemical processing (Robinson et
77 al., 2007; Lane et al., 2008).

78 Regional (Li et al., 2016; Akherati et al., 2019) and global models (Tsigaridis et al., 2014; Tilmes et al., 2019) have been
79 successfully used to simulate aerosol dispersion and chemical processing to some extent. However, they can be highly
80 uncertain (Bellouin et al., 2016; Johnson et al., 2020), particularly when comparing with on-site observations in a high time
81 resolution. This uncertainty can be due to a wide range of parameter settings, emission sources or missing processes, and is
82 challenging to comprehensively evaluate by only running direct model simulations, due to the computing time and expense
83 needed. Statistical analysis to evaluate model performance over parameter uncertainty can be made tractable through the use



84 of a statistical emulator (Carslaw et al., 2018). With a trained emulator, it is possible to study thousands or millions of model
85 variants (parameter combinations) and estimate the sources of uncertainty (Lee et al., 2011; Johnson et al., 2018; Wild et al.,
86 2020)

87 The VBS approach is often tuned to the environment of interest (Bergström et al., 2012; Shrivastava et al., 2013; Tilmes et al.,
88 2019; Shrivastava et al., 2019; Shrivastava et al., 2022) and, as mentioned before, doing this only with WRF-Chem runs is
89 particularly challenging and time consuming. The aim of this study is to determine an effective way of tuning the VBS scheme
90 using observations, and also to learn about the processes controlling OA in Delhi. Hence, we need to explore the combination
91 of different techniques, i.e., observations, WRF-Chem modelling with VBS implementation and statistical emulators, to better
92 understand the partitioning of matter between gaseous and particulate phases, and the chemical aging of POA. In this study, a
93 WRF-Chem parameterisation is proposed to simulate organic mass concentrations and organic to carbon (O:C) ratios over the
94 region of New Delhi, India, that includes detailed VBS and secondary organic aerosol (SOA) formation schemes. The model
95 performance is evaluated over a multi-dimensional parameter uncertainty space that explores parameter uncertainty in these
96 schemes. We generate a perturbed parameter ensemble (PPE) of 111 model runs that cover the model's uncertainty space and
97 compare output from each run to AMS observations of OA concentrations and O:C ratios measured at New Delhi, India. The
98 PPE is then used to construct statistical emulators and sample densely over the uncertainty for a more detailed comparison
99 over a specific time-period of the observations. The evaluation over specific time-periods will allow to study the behaviour of
100 the model setup under different conditions, i.e., high vs low mass concentrations, and analyse the impact the different parameter
101 setups have on the organic mass concentrations.

102 2 Methodology

103 2.1 WRF-Chem parameterisation and setup

104 The Weather Research and Forecasting model coupled with Chemistry (WRF-Chem) is used to simulate the emission,
105 transport, mixing, and chemical transformation of trace gases and aerosols concurrently with meteorology data (Grell et al.,
106 2005; Fast et al., 2006). Here, WRF-Chem version 3.8.1 is run with a 15 km domain, 55 x 55 grid cells, (Figure 1) and a
107 simulation period from 19th April - 29th May 2018, with substantial modification, details in below. This period was selected in
108 order to compare with aerosol measurements performed at New Delhi (Reyes-Villegas et al., 2021). Table 1 lists the
109 components that contribute to our model set-up, including the chemistry and aerosol schemes, emissions inventories and
110 boundary condition specifications. Gas-phase chemistry is simulated with the Common Representative Intermediates (CRI)
111 mechanism which permits a reasonably detailed representation of volatile organic compound oxidation. The aerosol chemistry
112 is simulated using the sectional MOSAIC module (Zaveri et al., 2008), including N₂O₅ heterogeneous chemical reactions
113 (Archer-Nicholls et al., 2014; Bertram and Thornton, 2009) and is coupled to the aqueous phase, which allows aerosols to act
114 as cloud condensation nuclei, as well as the removal of aerosols through wet deposition processes. The aerosol size distribution
115 in MOSAIC is described by eight size bins spanning a dry particle diameter range of 39nm to 10µm (Zaveri et al., 2008).

116 Table 1: WRF-Chem setup

Parameter	Set up
Gas phase mechanism	CRI-v2R5 (Watson et al., 2008; Archer-Nicholls et al., 2014)
Aerosol module	MOSAIC (Zaveri et al., 2008; Fast et al., 2006) with VBS (Shrivastava et al., 2011) with SOA (Tsimpidi et al., 2010)
Anthropogenic emissions	EDGAR-HTAP and SAFAR-India (CRI-v2R5 speciation)
Fire emissions	FINN 1.5 (Wiedinmyer et al., 2011)
Biogenic emissions	MEGAN (Guenther et al., 2006)
Chemical Boundaries	CESM2/WACCM (Danabasoglu et al., 2020)



Meteorological Boundaries | ECMWF Reanalysis (Hersbach et al., 2018)

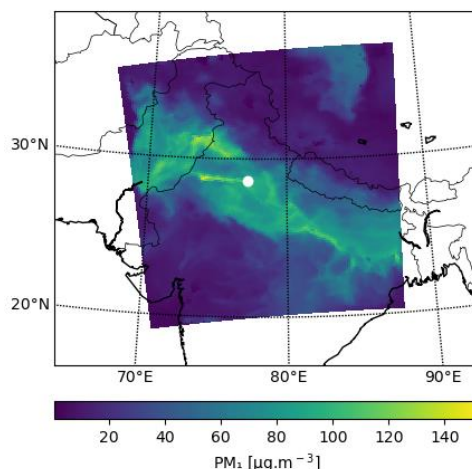
117

118 Our main modifications are focused on the treatment of the OA components. POA is treated as semi-volatile, using the VBS
119 treatment of Shrivastava et al. (2011). Their 9 volatility bin VBS scheme has been adapted for use in the 8 size bin version of
120 MOSAIC. Secondary organic aerosol (SOA) has been included based on the scheme described in Tsimpidi et al. (2010),
121 providing ‘anthropogenic’ (ARO1 and ARO2) and ‘biogenic’ (Isoprene and monoterpenes) SOA components, each covering
122 4 volatility bins. ARO1 represents the aromatics with OH reaction rates less than $2 \times 10^4 \text{ ppm}^{-1} \text{ min}^{-1}$, and ARO2 the aromatics
123 with OH reaction rates greater than $2 \times 10^4 \text{ ppm}^{-1} \text{ min}^{-1}$. Co-condensation of water has been added for these semi-volatile
124 organics, and they have been coupled to the aqueous phase in the same manner as other aerosol compounds in MOSAIC.
125 Previous studies have demonstrated that the condensation of semivolatile organic material onto aerosol particles substantially
126 increases the soluble mass of particles, their chemical composition and eventually their effective dry size (Topping et al., 2013;
127 Crooks et al., 2018).

128 Previous studies using the VBS have used scaling factors from POA to derive SVOC emissions in each volatility bin based on
129 equilibrium partitioning calculations, as well as volatility distributions based on laboratory studies and assumed oxygenation
130 and chemical reaction rates (Shrivastava et al., 2011; Fountoukis et al., 2014). To investigate the impact of these assumptions
131 on the model predictions, we have modified the model code so that the VBS emissions, the oxygenation rates and VBS reaction
132 rates, can be directly controlled via namelist options. The parameters which are perturbed in this way for this study are
133 described in more detail in Section 2.3.

134 The volatility distribution for biomass burning emissions is taken from May et al. (2013), and multiplied by a scaling factor of
135 3 (based on equilibrium partitioning calculations) to ensure reasonably similar condensed mass at emission as that reported in
136 the FINN 1.5 emission dataset. Similar calculations have been made in previous studies, giving roughly the same scaling factor
137 (Shrivastava et al., 2011; Fountoukis et al., 2014; Ciarelli et al., 2017). The volatility distribution for anthropogenic emissions
138 is also multiplied by a scaling factor of 3 for the same reasons as above. More information about the VBS distributions and
139 parameter space setup is in section S1 in the supplementary material.

140 Anthropogenic emissions are derived from the EDGAR-HTAP, SAFAR-India (CRI-v2R5 speciation) and NMVOC global
141 emission datasets, with NMVOC emissions speciated for the CRI-v2R5 chemical scheme, and applying diurnal activity cycles
142 to the emissions based on emission sectors in Europe (Olivier et al., 2003). We used these diurnal activity cycles (Figure S1
143 in supplement) as there were no data available for activity behavior in Delhi. Biogenic emissions are calculated online using
144 the MEGAN model (Guenther et al., 2006). Biomass burning emissions are taken from the FINNv1.5 global inventory
145 (Wiedinmyer et al., 2011).



146

147 Figure 1. WRF-Chem model domain with PM_{10} concentrations. White marker highlights the location of IMD New Delhi,
148 where the AMS observations were taken.



149 2.2 Observations

150 Aerosol observations were made at the Indian Meteorology Department (IMD) at Lodhi road in New Delhi, India (Lat 28.588,
151 Lon 77.217) from 26th April to 30th May 2018 as part of the PROMOTE campaign (Reyes-Villegas et al., 2021). A High-
152 Resolution Time-of-Flight Aerosol Mass Spectrometer (HR-TOF-AMS, Aerodyne Research Inc.), hereafter referred to as
153 AMS, was used to measure mass spectra of non-refractory particulate matter with an aerodynamic diameter equal or lower
154 than 1 μm (PM_{10}), including organic aerosols (OA), sulphate (SO_4^{2-}), nitrate (NO_3^-), ammonium (NH_4^+) and chloride (Cl^-), in a
155 5-minute time resolution. The AMS operation principle has been previously described by DeCarlo et al. (2006). The AMS was
156 calibrated during the campaign for the ionisation efficiency of nitrate (IE) and the relative ionisation efficiency (RIE) of other
157 inorganic compounds using nebulised ammonium nitrate and ammonium sulphate with a diameter of 300 nm. The data were
158 analysed using the IGOR Pro (WaveMetrics, Inc., Portland, OR, USA) based software SQUIRREL (Sequential Igor data
159 Retrieval) v.1.63I and PIKA (Peak Integration by Key Analysis) v.1.23I. The organic to carbon (O:C) ratios were calculated
160 with PIKA using the improved-Ambient elemental analysis method for AMS spectra measured in air (Canagaratna et al.,
161 2015). The AMS data, OA mass concentrations and O:C ratios, are used to compare with the WRF-Chem model outputs: total
162 organic matter mass concentration (Total_OM) and organic to carbon ratios (OC_ratio).

163 There were no Planetary boundary layer height (PBLH) measurements available at IMD Lodhi road, hence, PBLH data were
164 sourced from ECMWF ERA5 with 0.25 deg. results in 1-hour resolution for the coordinates closest to the IMD site.
165 Meteorology data was downloaded from <https://ncdc.noaa.gov/> (last access: 05/01/2019) for the Indira Gandhi International
166 Airport, India meteorology station.

167 The meteorology data were used to interpret the diurnal behaviour of the chemical species and to compare with meteorology
168 outputs from WRF-Chem. A dataset of meteorology was not available at IMD. The use of meteorology from airports has been
169 previously used and is considered to be representative of regional meteorology without being affected by surrounding buildings
170 (Reyes-Villegas et al., 2016).

171 2.3 Perturbed Parameter Ensemble

172 To evaluate the sensitivity to variations in the VBS emission and processing parameters of our WRF-Chem model of the
173 simulated OA over the New Delhi region, we generated a perturbed parameter ensemble (PPE). We choose a set of simulations
174 with optimal space-filling properties that provide effective coverage across the multi-dimensional space of the uncertain model
175 parameters. Here, we perturb ten parameters of the WRF-Chem model that relate to OA emissions and the aging of these VBS
176 compounds. The parameters correspond to five processes in the model, which are perturbed with respect to both anthropogenic
177 emissions and biomass burning emissions. These process parameters are:

- 178 1. **VBS ageing rate:** The reaction rates of VBS compounds with OH - each reaction reduces the volatility of the
179 compound by a factor of 10 (1 decade in saturation concentration, Ci^* , position), and adds 7.5% oxygen. Ci^* is the
180 condensed mass loading at which half of the organic material in that volatility bin will be in the condensed phase, and
181 half will be in gas phase (Donahue et al., 2006).
- 182 2. **SVOC volatility distribution:** This parameter is expressed in terms of an “equivalent age”, determined using a simple
183 ageing model. At time = 0 all VBS molecules will be highly volatile, with a $\text{Ci}^* = 4$. These compounds are processed
184 at a fixed reaction rate (at each step 0.1% of the gaseous mass in a volatility bin is moved to the next volatility bin),
185 with simple equilibrium partitioning of the VBS components between the gas and condensed phases (to roughly
186 simulate the manner in which VBS compounds are partitioned and aged within the WRF-Chem scheme). This
187 processing reduces the overall volatility of the VBS compounds, first providing a spread of mass across the volatility
188 range, before accumulating the mass in the lowest volatility bins until 90% of the VBS mass is in the $\text{Ci}^* = -2$ volatility
189 bin (“time” = 1). This parameter is a scalar variable (between 0-1), that indicates the dimensionless position between
190 these two points, and has an associated volatility distribution. After examining the range of volatility distributions



191 given by this simple ageing model, we have chosen to use distributions within the range of 0.05 to 0.4. Using values
192 above 0.05 ensures there will always be some lower volatility compounds to condense. Above 0.4 almost everything
193 is condensed, so we have excluded values above this so that our PPE does not become too heavily weighted towards
194 these scenarios. Example volatility distributions across the chosen range are shown in supplementary figure S2.

- 195 3. **SVOC oxidation rate:** This parameter represents the degree of oxidation that occurs with (or is induced by) each
196 reaction with an OH molecule. Previous studies have used values between 0.075 (7.5%) extra oxygen (or one oxygen
197 atom) (Robinson et al., 2007) and 0.40 (40%) extra oxygen (or five extra oxygen atoms per reaction) (Grieshop et
198 al., 2009). Grieshop et al. (2009) stated that with 7.5%, there is not enough addition of oxygen to the organic mass,
199 while with the 40% there is a noticeable improvement to the OA oxygen content with little effect on the predicted
200 organic mass production. In our study, the lowest level is 0.075 extra oxygen (or one oxygen atom) and the uppermost
201 level is 0.45 (or six extra oxygen atoms per reaction).
- 202 4. **IVOC scaling:** IVOC compounds bridge the gap from SVOC to VOC ($\log_{10}(C^*)$ 4-6). Including the IVOC
203 independently to parameter (2) (based on our simple ageing model) enables us to still include these within the
204 volatility distribution (this does restrict the impact of parameter (2) to influencing the shape of the volatility
205 distribution for the lower C^* values only. These IVOC emissions are calculated using a fixed volatility distribution
206 which scales from the non-volatile OA mass in the emissions inventory. The fractional emitted masses are: 0.2 for
207 $C_i^* = 4$; 0.5 for $C_i^* = 5$; and 0.8 for $C_i^* = 6$ (as shown in supplementary Figure S2). These fractions are then adjusted
208 by this scaling factor, in the range 0-3.
- 209 5. **SVOC scaling:** This parameter is the scaling factor of the SVOC emissions, (which have been given a volatility
210 distribution by parameter 2). Traditionally such scaling has been used: to ensure that the condensed mass of the
211 emitted SVOC is the same as the non-volatile OA mass in the emissions inventory; however, this scaling could also
212 be used to off-set errors in the emission inventory estimates of OA emissions. The scaling needed to ensure that the
213 emitted condensed mass is the same will never be less than 1, but could go to x20 (or more) for the "younger" SVOC
214 volatility ranges (as estimated using the equilibrium partitioning tool for parameter 2). However, in order to
215 accommodate potential over-estimates of the emission inventories, and to avoid too much OA being generated after
216 aging of any highly-volatile emissions, we chose an SVOC scaling range 0.5 to 4.

217 Table 2 shows the uncertainty ranges applied to each of the parameters, that we explore with the PPE, and Table S1 in the
218 supplementary information shows an example of a 'namelist.input' file with the parameters to control the VBS scheme, that
219 was used to create the model simulation. A total of 111 model simulations make up the ensemble. Following the statistical
220 methodology outlined in Lee et al. (2011), the combinations of input parameters used for the simulations in the PPE were
221 selected using an optimal Latin hypercube statistical design algorithm (Stocki, 2005), providing a good coverage of the multi-
222 dimensional parameter space. The selection of combinations was performed in three subsets, for use in building statistical
223 emulators to densely sample key outputs from the model over its uncertainties. First, a single design of 61 runs was generated
224 for training the emulators (subset 1), and then a second set of 20 runs was made that 'augmented' into the larger gaps of the
225 first design, for use in validating the emulators (subset 2). On an initial comparison to observations, the observations were
226 found to be outside the range of the PPE's output, and following an investigation into this, the lower bound of the anthropogenic
227 SVOC scaling parameter (parameter 5) was extended from 0.5x down to 0.1x. Hence, an extra, third, set of 30 runs were
228 designed and simulated to cover the extended parameter space (subset 3), leading to a total of 111 runs in the final PPE. Table
229 S2 in supplementary information provides a list of the model runs that make up the PPE.

230 Table 2: Range of the parameter space used in the PPE with 111 model variants.

Parameter number	Parameter name	min	Max
1	Anthropogenic VBS ageing rate	1.00E-13	1.00E-11
2	Anthropogenic SVOC volatility distribution	0.05	0.4



3	Added oxygen per generation of ageing	0.075	0.45
4	Anthropogenic IVOC scaling	0	3
5	Anthropogenic SVOC scaling	* 0.1	4
6	Biomass Burning VBS ageing rate	1.00E-13	1.00E-11
7	Biomass Burning SVOC volatility distribution	0.05	0.4
8	Added oxygen per generation of ageing	0.075	0.45
9	Biomass Burning IVOC scaling	0	3
10	Biomass Burning SVOC scaling	0.5	4

231 * 81 runs were performed with an anthropogenic SVOC scaling min = 0.5 and max = 4 and 30 runs were performed with an
232 anthropogenic SVOC scaling min = 0.1 and max = 0.5. This due to a min = 0.5 and max = 4 giving high Org mass
233 concentrations, when compared with AMS.

234 2.4 Emulation

235 For each PPE member, a time series of the OC_ratio and Total_OM from the WRF-Chem model run was extracted at the
236 closest coordinates to the IMD site (Lat 28.628, Lon 77.209) in the model output. Gaussian process emulators (O'Hagan,
237 2006; Lee et al, 2011) were built using the PPE. Similarly to the approach described in Johnson et al. (2018), initial emulators
238 were constructed using only training simulations (subsets 1 and 3) and these were validated using the validation runs (subset
239 2). Once validated, a further new emulator was then constructed using both the training and validation simulations of the PPE
240 together as training data, to obtain a final emulator based on all of the information that the PPE contains. An additional
241 verification of the quality of each final emulator was obtained via a 'leave-one-out' validation procedure (where each
242 simulation in turn is removed from the full set of 111 runs and a new emulator is built and used to predict that removed
243 simulation).

244 Monte Carlo sampling of the emulators enabled dense samples of model output to be generated over the 10-dimensional
245 parameter uncertainty of the model. We produced output samples for a set of 0.5 million input parameter combinations across
246 the uncertainty space, hereafter called 'model variants', to explore the model's uncertainty.

247 2.5 Model evaluation

248 Alongside the emulation, outputs from the 111 model runs (OC_ratio and Total_OM) were additionally evaluated, against the
249 AMS observations (O:C and OA), using various model evaluation tools, including the fraction of predictions within a factor
250 of two (FAC2), mean bias (MB) and the index of agreement (IOA). Section S2 of the supplementary information provides a
251 detailed explanation of the calculations for each evaluation metric and information on how to interpret the values.

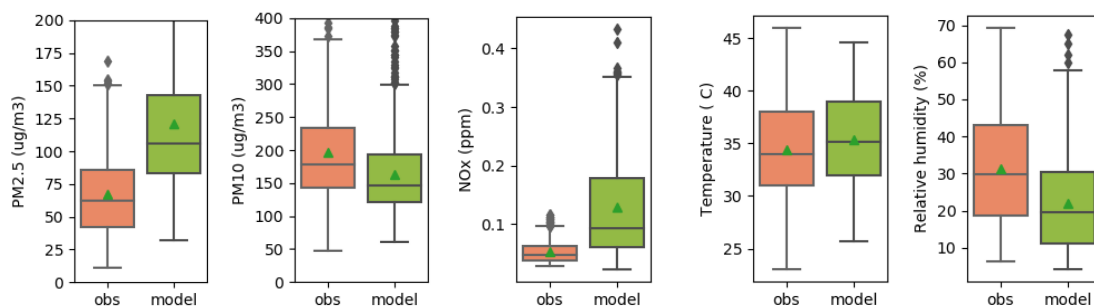
252 3 Results and discussion

253 3.1 Model outputs and observational analysis

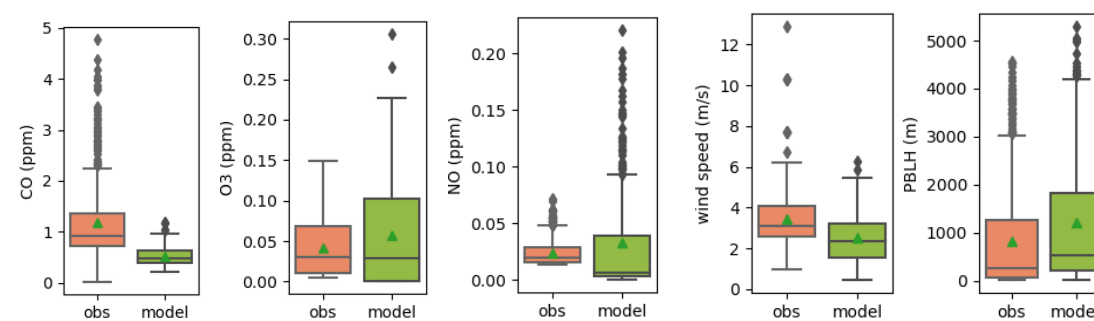
254 The model outputs of the central WRF-Chem run, from the original parameter space (Subsets 1 and 2), are used to compare
255 with observations in order to analyse the model performance. As mentioned in the methods section, the VBS setup will affect
256 OA concentrations and PM, with no implications to inorganic aerosols or gaseous species. Figure 2 shows the comparison for
257 the full dataset (1st – 29th May 2018) between model outputs and observations performed at IMD Lodhi road, where we see
258 higher PM_{2.5} and NO_x concentrations in the model simulation. The high NO_x concentrations in the model seem to be related
259 to high NO₂ concentrations as the NO concentrations are in line with the range of the observations of NO. Looking at the
260 meteorological parameters, we can see similar temperatures and wind speeds between the model and observations, with lower
261 RH and higher PBLH in the model.



262



263

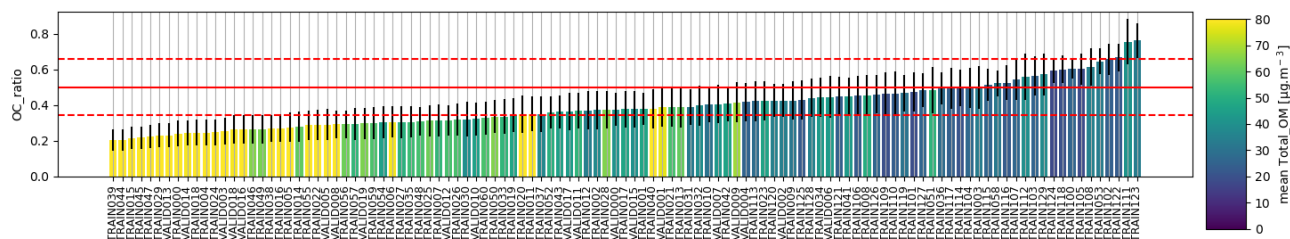


264 Figure 2. Comparison of observations (At Lodhi Road for air quality and IGI Airport for meteorology parameters) and model
 265 outputs of various parameters. May 2018. Bars highlight medians, quartiles and 95%, triangles highlight the mean.

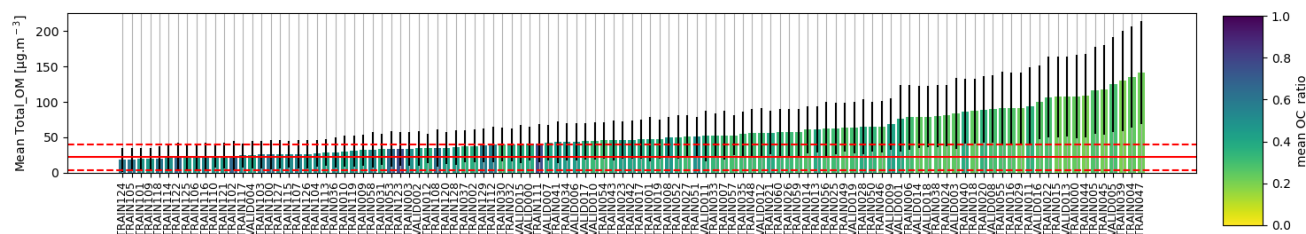
266 **3.2 Model runs and AMS observations**

267 Here, we analyse and compare the mean values of Total_OM and OC_ratio for the full period, 1st – 29th May 2018, of the 111
 268 WRF-Chem model runs (Table S2 in supplement) with the AMS observations (OA and O:C). The top panel in figure 3 shows
 269 a bar plot of the mean OC_ratio for the model runs coloured by the mean total_OM concentrations. The bottom panel shows
 270 the mean total_OM concentrations for the model runs coloured by the mean OC_ratio. The model runs are sorted from low to
 271 high values of the y-variable. The continuous and dashed red lines show the mean \pm one standard deviation (SD) of the O:C
 272 ratio (top) and OA (bottom) measured with the AMS. In general, compared to mean values measured with the AMS, a large
 273 number of WRF-Chem runs had a low O:C_ratio and high mean Total_OM concentrations. The bottom panel shows the mean
 274 total_OM concentrations of 47 runs lay within one SD of the mean OA concentration of $21.77 \mu\text{g}\cdot\text{m}^{-3}$ measured with the AMS.
 275 Moreover, the model runs with mean Total_OM concentrations near the mean OA concentrations have OC_ratio mean values
 276 near the O:C mean AMS value (0.5), with a cyan colour. This analysis shows a number of model runs with mean Total_OM
 277 and OC_ratio values near the mean values measured with an AMS.

278



279



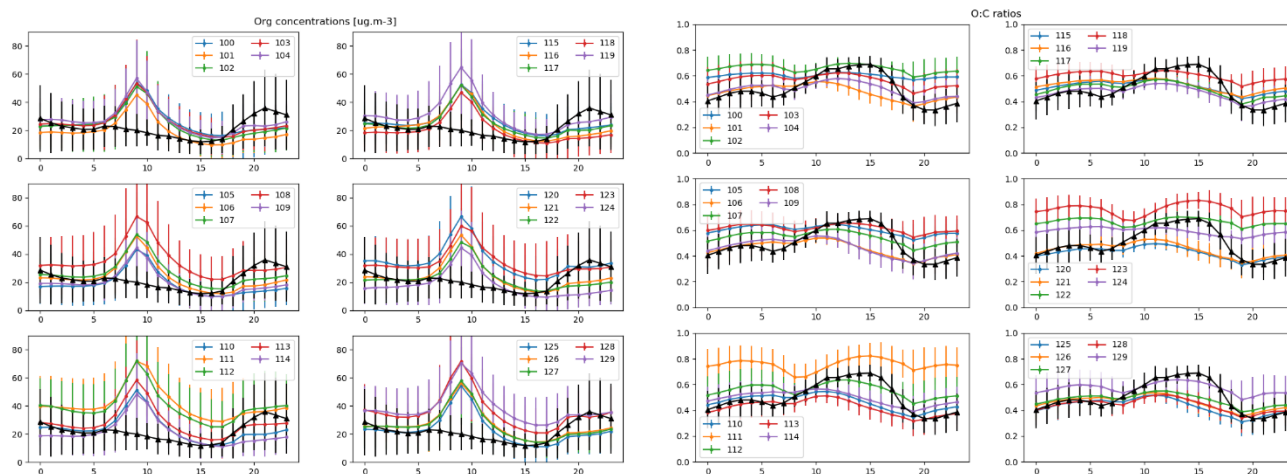
280

281 Figure 3. Analysis of the 111 model runs for the full period. Mean OC_ratio coloured by mean Total_OM (top plot) and
282 mean Total_OM coloured by mean OC_ratio (bottom plot). The red lines highlight the mean \pm SD of AMS observations
283 (O:C top and OA bottom). The mean AMS values are O:C = 0.5 and OA = 21.77 $\mu\text{g.m}^{-3}$.

284 3.3 Diurnal analysis to WRF-Chem runs

285 The high time resolution data collected with the AMS provides the opportunity of analysing the WRF-Chem outputs in more
286 detail, for example by looking at the diurnal cycles. Figure 4 shows the diurnal cycles of chosen WRF-Chem runs with
287 Total_OM concentrations and OC_ratio close to the AMS observations. In the model runs, we were able to span high and low
288 Total_OM and OC_ratio. However, in the case of OC_ratio, we were not able to span the range of the O:C from AMS
289 observations with mean values of 0.3 at night and 0.7 during the day. Looking at the Total_OM concentrations, we identified
290 two potential structural errors in the WRF-Chem outputs, the early morning peak and the late evening low concentrations. This
291 could be due to application of unsuitable diurnal activity cycles to the emissions or WRF-Chem not being able to capture
292 completely the dynamics of the planetary boundary layer. With no activity data available for Delhi, we used diurnal cycles of
293 activities based on emission sectors in Europe (Olivier et al., 2003) (Figure S1 in supplement). For the diurnal cycles of
294 meteorology (Figure S4), we can see that the model agrees with the PBLH- ERA5 in the early morning and until 14:00 h, time
295 when PBLH- ERA5 starts dropping and PBLH-Model remains high, perhaps preventing concentrations to accumulate. This
296 makes building and testing the emulator challenging as we may get the correct concentrations for the wrong reasons. The
297 emulator can be built over a specific time-period and be compared with the observations. Hence, the emulator was built over
298 two periods of interest; the full period (1st-29th May) and a period where no potential structural errors were identified from
299 14:00- 16:00 hrs for 1st-29th May (2-4 pm period). Emulator analysis involving the filtering of model results to avoid structural
300 errors has been successfully performed previously in constraining a climate model (Johnson et al., 2020). Looking at the mean
301 OC_ratio and Total_OM of the model runs for the 2_4 pm period (Figure S6), 34 runs lay within one SD of the OA mean
302 concentration (12.20 $\mu\text{g.m}^{-3}$) measured with the AMS, compared with the 47 runs identified from figure 3. This means that
303 even by analysing the 2-4 pm period we still have model runs that cover the AMS observations.

304



305

306 Figure 4. Diurnal cycle of selected WRF-Chem runs with values near the AMS observations (black line).

307 3.4 Model evaluation

308 There are various tools that can be used to compare the model outputs with the observations. In this study, we use a number
309 of statistical metrics (see Section S3 in the supplementary information for a detailed description of each metric we consider)
310 to evaluate the ensemble of 111 model runs for the 2-4 pm period and the full period. The fraction of predictions within a
311 factor of two (FAC2) represents the fraction of data where predictions are within a factor of two of observations. The Mean
312 Bias (MB) gives an indication of the mean over- or under-estimation of predictions. The Index of Agreement (IOA) is a
313 commonly used metric in model evaluation (Willmott et al., 2012), ranging between -1 and +1, with values close to +1
314 representing a better model performance. Table S3 shows the results of the model evaluation for the 2-4 pm period and table
315 S4 the results for the full period. When comparing the performance of the two periods; the model runs of the 2-4 pm period
316 have a better performance with 103 runs for O:C and 29 runs for OA with $FAC2 > 0.6$ compared to 94 runs for O:C and 4 runs
317 for OA with $FAC2 > 0.6$ for the full period. The negative MB in O:C suggests the models are underestimating the O:C ratios
318 (between -0.01 to -0.15) measured with the AMS. However, the FAC2 values of 0.96 and higher indicate that the models are
319 doing a good job overall at simulating the O:C ratios. This is not the same for OA concentrations, where the models show an
320 over-estimate of the concentration compared to observations, and where only 0.56 -0.62 of predictions were within a factor of
321 two of the OA observations.

322 The IOA provides similar results with a better model performance in the 2-4 pm period, with 10 model runs for the 2-4 pm
323 period and only two runs for the full period with IOA values equal or higher than 0.45. It is interesting to see that while FAC2
324 was higher, for OA and O:C, in the 2-4 period runs compared to the full period, IOA values in 2-4 period were high with OA
325 but low with O:C, which reached IOA values of 0.53 in the 2-4 period and 0.56 in the full period. Previous studies performing
326 modelling evaluation determined similar IOA values using various models (Ciarelli et al., 2017; Fanourgakis et al., 2019). For
327 instance, Chen et al. (2021), modelling SOA formation, obtained IOA between 0.39 – 0.49. Huang et al. (2021) published
328 recommendations on model evaluation and identified IOA of around 0.5 for organic carbon. Lee et al. (2020) performed a
329 sensitivity analysis to two different SOA modules and obtained IOA values of 0.46 – 0.52.

330 The model evaluation metrics, along with the parameter setup for each ensemble member, allow us to analyse the model setup
331 that gives a better performance. Figure 5 shows the relative variation (%) of the five anthropogenic parameters of the PPE (1
332 – 5) for the 2-4 pm period (Figure S7 in supplementary material shows the analysis for the full period). Each pentagon
333 represents the 5-D parameter space and the positions of the dots connected with lines show the position of each parameter



334 within its range for that specific ensemble member. The filled area within the dots represents the explored parameter space in
335 each ensemble member. We are analysing the five anthropogenic PPE only since the five parameters related to biomass burning
336 represented a low contribution to the Total_OM concentrations. We are looking for blue, light blue or green colours in the
337 lines and dots (high FAC2 values from the O:C analysis) and blue, light blue or green colours in the filled area (high FAC2
338 values from the OA analysis) to identify the model runs with a good evaluation. In figure 5, we can see that the best runs
339 according to the O:C and OA model evaluation are TRAIN127 and TRAIN121 with other TRAIN runs also with good
340 performance such as (126, 036, 117, 104, 115, 119 and 058). In general, these model runs have low SVOC volatility distribution
341 and SVOC scaling. TRAIN127 and TRAIN121 have low VBS ageing rate, SVOC volatility distribution and SVOC scaling
342 and with either high SVOC Oxidation rate or high IVOC scaling.



343



344

345 Figure 5. Relative variation (%) of the 5 anthropogenic PPE (1 – 5) for the 2-4 pm period. Each pentagon represents the 5-D
346 parameter space and the positions of the dots connected with lines show the position of each parameter within its range for
347 that specific ensemble member. The filled area within the dots represents the explored parameter space in each ensemble
348 member. Anticlockwise from top there are the five anthropogenic parameters: VBS ageing rate (1), SVOC volatility
349 distribution (2), SVOC Oxidation rate (3), IVOC scaling (4) and SVOC scaling (5). The values of the 5 parameters have been
350 normalised dividing by their respective maximum values, hence their values in this plot range from 0 – 1. Example of
351 interpretation in bottom right: the five parameters are towards their high values = 1.0. The colour in the lines and dots represents
352 the FAC2 values from the O:C analysis and the fill colour represents the FAC2 values from the OA analysis. Red = 0 – 0.2,
353 orange = 0.2 – 0.4, yellow = 0.4 – 0.6, green = 0.6 – 0.8, light blue/cyan = 0.8 -0.9 and blue = 0.9 -1.0



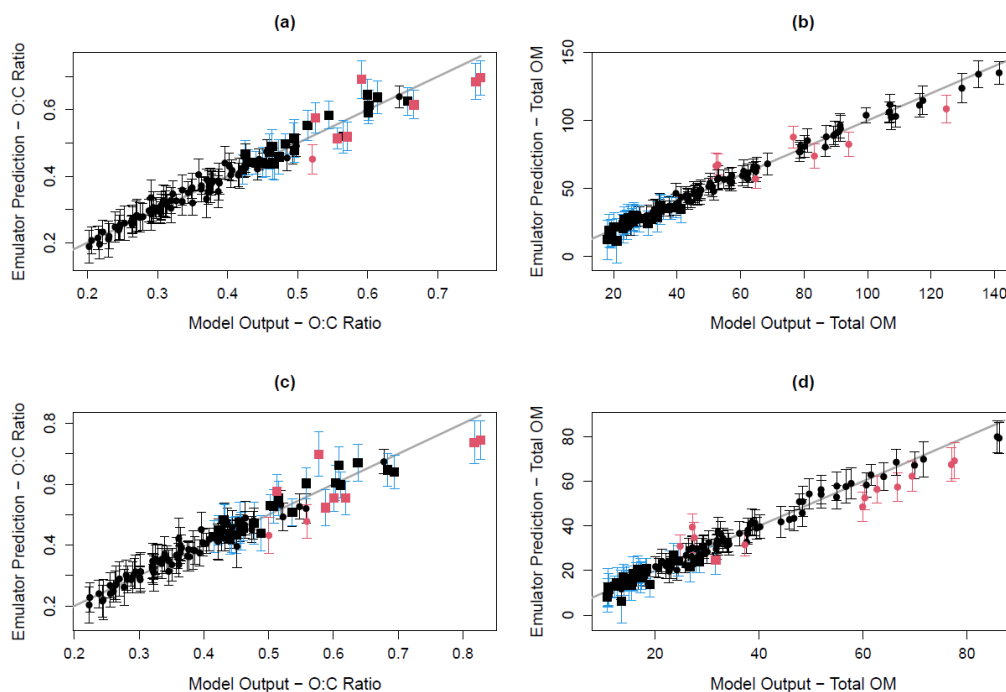
354 3.5 Emulator analysis

355 3.5.1 Emulator building and testing

356 Once we confirm that the ensemble of 111 model runs span the AMS observations we can use it to build the emulator. The
357 emulators are tested using the leave-one-out validation approach (Johnson et al., 2018). In this analysis, each ensemble run is
358 first excluded from the emulator build, and then the emulator is used to predict the output at the parameter setting of the
359 excluded run. Figure 6 shows plots of the emulator predictions (with 95% credible intervals from the emulator model) vs the
360 model outputs of the 111 runs from the leave-one-out validation for OA. Predictions from a perfect emulator would follow
361 exactly along the 1:1 line on the plots.

362 We built and tested the emulator for the full period (1st – 29th May) to have an overview of the emulator performance. The
363 emulator can be built over a specific time-period to compare with the observations. This allows to study the model performance
364 under different conditions, i.e., high/low aerosol concentrations, day/night, etc. We selected four period time-slots to build and
365 test the emulator under high and low Total_OM concentrations and two time-slots. These four emulators showed a good
366 validation analysis (Refer to section S5.1.1 in the supplementary material). However, due to the potential structural errors
367 identified from the diurnal analysis (Section 3.3), we will focus on the selected period without structural errors, 2-4 pm period.
368 Figures S11 and S12 in supplementary material show the spread of Total_OM and OC_ratio respectively, for the ensemble of
369 111 model runs vs the 10 parameters.

370 We see in Figure 6 that overall, the emulators built for the two periods; full period (6.a and 6.b) and 2-4 pm period (6.c and
371 6.d) show a good performance; For the 2-4 pm period, Total_OM with only nine runs that are not within the 95% CI from
372 prediction (red markers) and OC_ratio with ten runs that are not within the 95% CI from prediction. With the new 30 runs
373 (error bars in blue) we managed to reduce the Total_OM concentrations with good prediction on the emulator. However, there
374 is a compromise in the OC_ratio with eight runs with high OC_ratio values that are not within the 95% of the prediction interval
375 of the emulator.



376



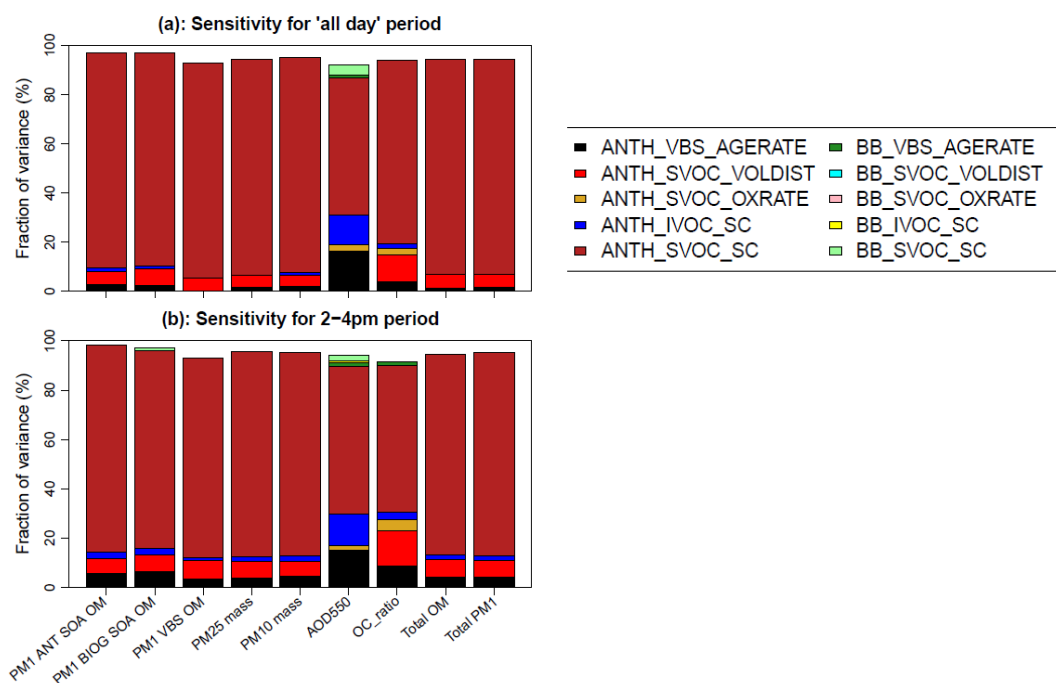
377

378 Figure 6. Validation of the full (a and b) and 2-4 pm (c and d) periods for O:C ratio and Total OM. Circles are the original 81
379 runs. Squares with error bars in blue are the new 30 runs with low settings of the anthropogenic SVOC scaling parameter
380 (which has led to low aerosol mass). Runs where the actual model output lies outside the 95% prediction interval of the
381 emulator are shown in red.

382 3.5.2 Emulator sensitivity analysis

383 We use a variance-based sensitivity analysis (Lee et al., 2011; Johnson et al., 2018) to decompose the overall variance in the
384 model output for key variables of interest into percentage fractions for the 10 parameters. This analysis was performed to the
385 full period and the 2-4 pm period (Figure 7). Looking at the parameters for the two periods, the anthropogenic SVOC scaling
386 has the highest contribution to the variance, which suggests that constraining this parameter would lead to a reduction in the
387 uncertainty in these outputs from the model. Anthropogenic SVOC volatility distribution has some impact on O:C ratios with
388 a fraction of variance of around 15%.

389



390

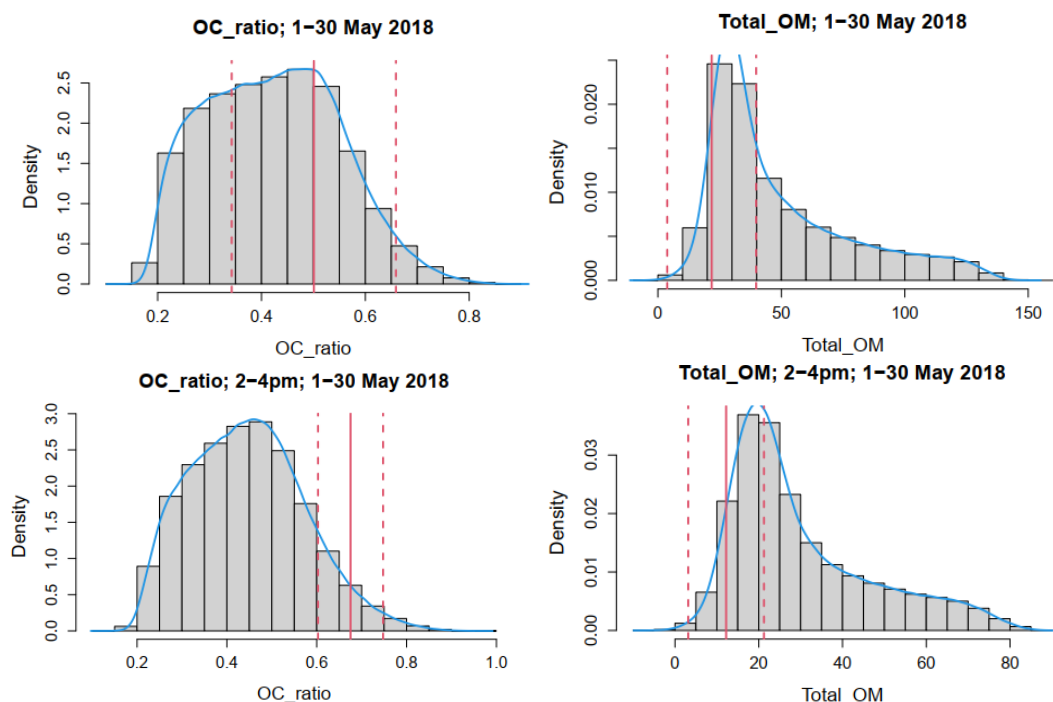
391 Figure 7. Sensitivity evaluation of the 10 chosen parameters for the 2-4 pm period (a) and the full period (b).

392 3.5.3 Impact of constraint on uncertainty

393 The emulator was used to predict model outputs for a sample of size 0.5 million, for the full period and the 2-4 pm period.
394 Figure 8 shows the probability distribution of OC_ratio and Total_OM predicted over the full parameter uncertainty. The
395 AMS mean \pm 1SD are shown in red. We can see the higher density (lower values) of the Total_OM show a good agreement
396 with the AMS-OA concentrations. However, in the case of O:C, the higher density lies on the low O:C ratios compared to the
397 O:C-AMS observations which lie in the upper tail of the predicted distribution. The OC_ratio varies within the two periods,
398 with a wider density range for the full period, 0.25-0.55, which represents the variability of the OC_ratio over the full day. In
399 the case of the 2-4 pm period, we can see more narrow density, 0.3-0.5, which, while lower than the mean O:C ratio measured



400 with the AMS (0.65), may be representative of the O:C ratios estimated with the WRF-Chem runs. This suggests that when
401 analysing diurnal behaviour of WRF-Chem outputs without structural errors, we would be able to analyse more into detail the
402 WRF-Chem performance over different hours of the day.



403 Figure 8. 0.5 million emulator sample, before constraint, covering the full parameter uncertainty space of the model for the
404 full period (a and b) and for the 2-4 pm period (c and d). Red highlights the AMS mean +/- SD observations.

405 3.5.4 Constraint effect.

406 The AMS observations, OA concentrations and O:C ratios, are used to constrain the emulation, applying an observation
407 uncertainty as mean \pm SD. With mean as the emulator prediction and 1 SD uncertainty, we apply the constraint when
408 accounting for emulator prediction uncertainty, by retaining the variant if the range mean \pm SD overlaps with the observation
409 uncertainty range.

410 Figure 9 is a 2-d histogram for joint constraint (Total_OM and OC_ratio) for the 2-4pm period, with colour showing frequency
411 of variants in a pixel of an underlying grid arranged as a pairwise (shown by the label box on each axis (above/to right)). Each
412 2-d pairwise space has been split into a 25x25 uniform grid to calculate the frequencies. Where the plots show yellow to red,
413 more variants are retained than in the green / blue areas, highlighting the most likely (higher probability) area of space. This
414 analysis shows that when constraining both Total_OM and O:C ratios, the emulator retains 52310 variants from 0.5 million,
415 which is approximately a 10.46% of the original variants generated. Figure S13 shows the histogram for the full period.

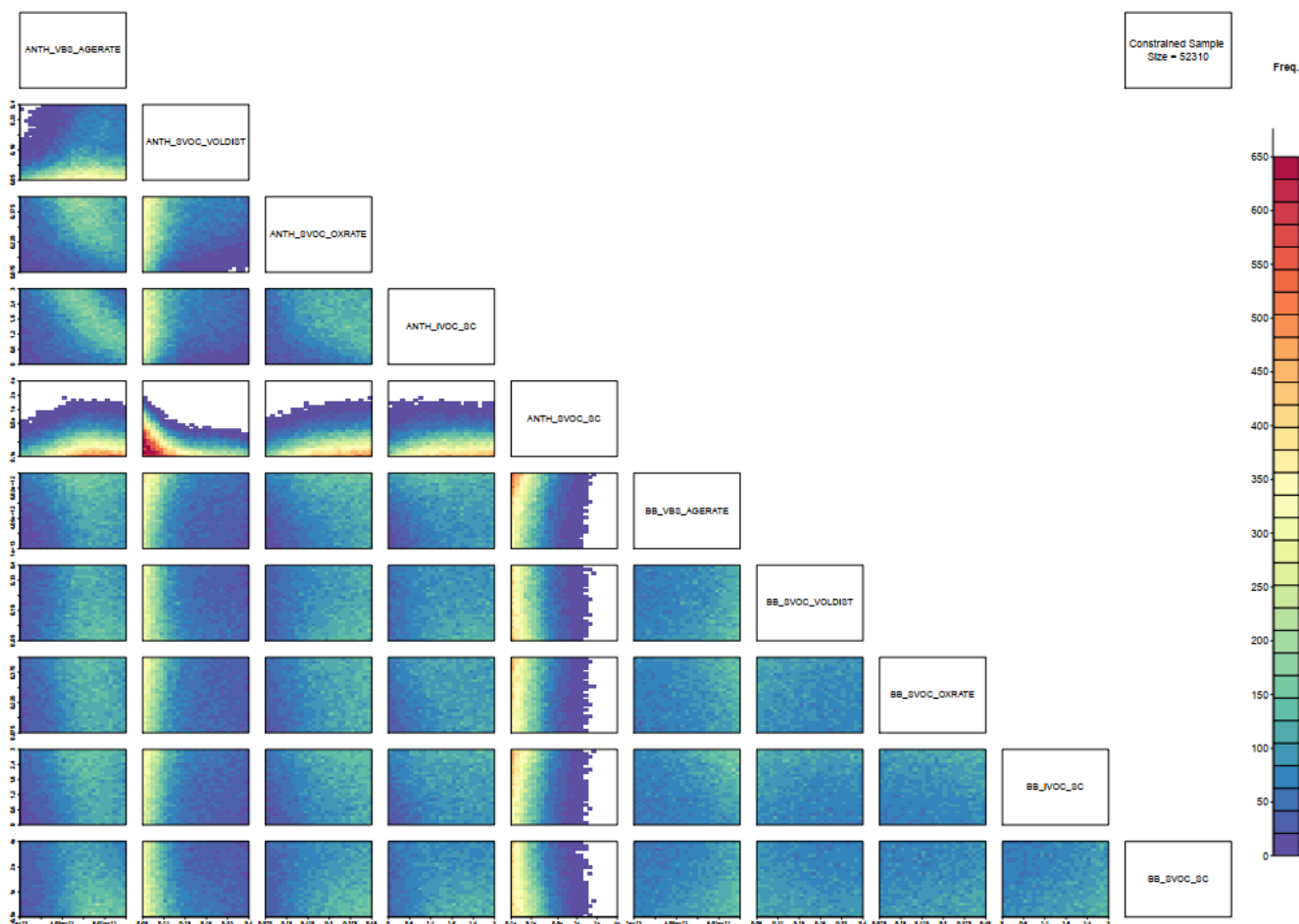
416 White areas indicate no variants at all retained in that pixel, so that 2-d space is ruled out with respect to all 10 dimensions.
417 (probability=0). Where the colour is uniform, e.g., biomass burning parameter plots in figure 9, the parameter is essentially
418 un-constrained, and all parts of parameter space with respect to those 2 parameters are equally likely/covered by variants (as
419 it was before the constraint was applied). These plots show where in parameter space is most likely given the comparison to
420 observation. These are the variants that we cannot rule out (are plausible) given the uncertainty – it does not mean they are all



421 ‘good’. It is worth mentioning that with this analysis we do not locate the exact ‘best’ run, we provide a range of potential
422 combinations to test the WRF-Chem set-up.

423 These results agree with the analysis in the model evaluation (Section 3.4). Figure 9 shows, in red colour, the higher probability
424 that with low SVOC volatility distribution and low SVOC scaling would give a good model performance. However, there is
425 no clear pattern with the other parameters.

426



427

428 Figure 9. 2-d histogram for joint constraint effect (Total_OM and OC_ratio) accounting for emulator uncertainty. Retain
429 52310 variants from 0.5 million emulations (~10.46%).

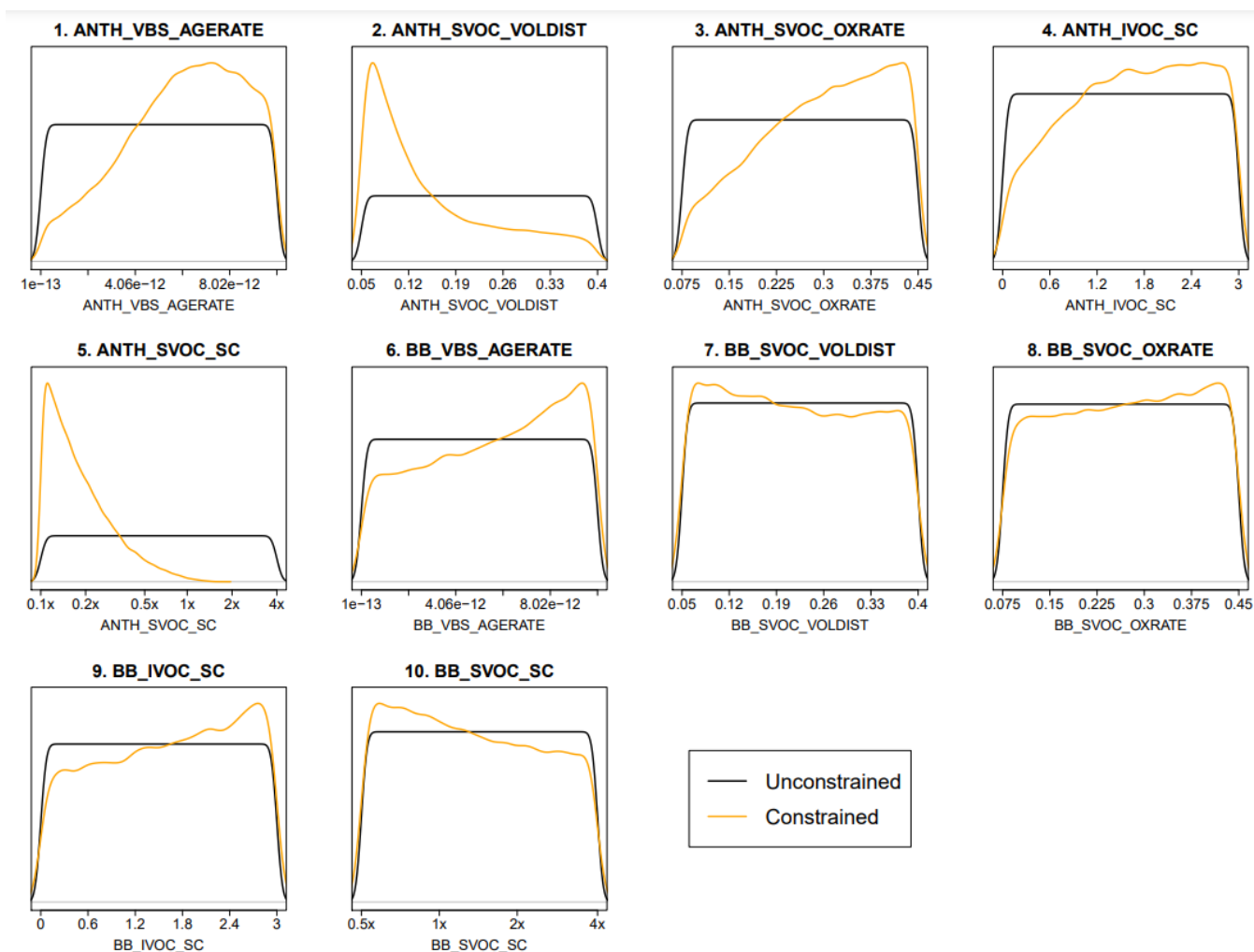
430

431 3.5.5 Marginal parameter constraints.

432 These plots show the marginal constraint (1-d projection) on the parameters over their ranges. The unconstrained sample
433 (black) has even coverage (is sampled uniformly) across all parameter ranges and the parameter space. The unconstrained
434 sample covers the full 10-d space.



435 Where the probability density function (pdf) of the constrained sample is above the black unconstrained pdf, this means the
436 likelihood of the parameter taking a value at that point of its range is increased on constraint (more probability). Where it is
437 below, it is now less likely on constraint (less probability). The more ‘squashed’ the unconstrained distribution is – the more
438 the likelihood of the parameter taking values in the range with higher density is. This analysis is a useful tool to identify the
439 more likely values of the 10 parameters over all the parameter space. Here, we can see that low SVOC volatility distribution
440 and low SVOC are clear parameter values that we can use to improve the WRF-Chem model setup. Other parameters that we
441 can start testing on WRF-Chem are; high BB VBS ageing rate (6) and BB IVOC scaling (9). It is worth highlighting the
442 similarity of the effects on the anthropogenic and biomass burning parameters.



443
444 Figure 10. Marginal Parameter Constraints: joint constraint effect (Total_OM and OC_ratio).
445

446

447

448



448 **3.6 Analysis of model evaluation and emulator runs.**

449 Table 4 shows the WRF-Chem runs with both mean Org and mean O:C values close to AMS observations for the two periods
 450 and also selected runs from the 2-d histograms (Figure 9). Here we can see a couple of interesting findings. First, the O:C
 451 ratios presented a better performance with the model evaluation metrics; FAC2 values higher than 0.9 compared with FAC2
 452 values up to 0.73 for the Total OM. Looking at the Total OM, there are higher FAC2 values in the 2-4 pm period, which might
 453 be related to the structural errors impacting the model performance in the full period. The MB provides an estimation of the
 454 over prediction of the Total_OM. In this study, WRF-Chem runs were in general overpredicting the Total OM concentrations.
 455 Hence, MB is an important metric. In both periods, there are runs where the overprediction was $5 \mu\text{g.m}^{-3}$ or lower, i.e.,
 456 TRAIN110, TRAIN121, TRAIN117, etc. This highlights the use of all the analysis presented in this study where we are able
 457 to identify probable values for the VBS model parameters and be able to model Total OM and O:C ratios.

458 Table 3. Analysis of model evaluation metrics and comparison with observations for the full and 2-4 pm periods. The FAC2
 459 ranking is based on high FAC2 values of the Total_OM analysis. Mean AMS values for the full period: OA = $21.77 \mu\text{g.m}^{-3}$
 460 and O:C = 0.5. Mean AMS values for 2-4 pm period: OA = $12.20 \mu\text{g.m}^{-3}$ and O:C = 0.67.

Full period		Total_OM					O:C ratio					
model	FAC2 ranking	FAC2	MB	IOA	Total_OM mean	Total_OM SD	FAC2 ranking	FAC2	MB	IOA	O:C ratio mean	O:C ratio SD
TRAIN110	1	0.62	2.23	0.45	23.75	16.58	27	0.94	-0.04	0.48	0.46	0.12
TRAIN126	2	0.61	5.13	0.38	26.42	19.83	20	0.95	-0.04	0.51	0.46	0.11
TRAIN119	5	0.60	9.54	0.31	30.83	22.05	7	0.97	-0.04	0.54	0.47	0.10
TRAIN117	6	0.59	3.18	0.41	24.56	16.93	10	0.97	-0.01	0.53	0.49	0.11
TRAIN009	8	0.59	10.54	0.30	68.50	36.13	15	0.96	-0.08	0.51	0.42	0.11
TRAIN121	9	0.59	2.87	0.41	24.17	18.59	21	0.95	-0.05	0.50	0.45	0.11
TRAIN104	11	0.58	5.77	0.39	24.17	18.59	8	0.97	-0.01	0.56	0.45	0.11
VALID002	12	0.58	13.27	0.24	34.49	24.15	2	0.98	-0.08	0.52	0.43	0.09
TRAIN003	13	0.57	12.65	0.24	33.73	23.56	6	0.97	0.00	0.55	0.50	0.12
TRAIN127	16	0.56	4.78	0.37	26.12	20.02	5	0.97	-0.02	0.55	0.48	0.10
2-4 pm period		Total_OM					O:C ratio					
model	FAC2 ranking	FAC2	MB	IOA	Total_OM mean	Total_OM SD	FAC2 ranking	FAC2	MB	IOA	O:C ratio mean	O:C ratio SD
TRAIN127	1	0.73	4.37	0.44	15.64	10.72	3	0.99	0.02	0.51	0.50	0.06
TRAIN121	3	0.72	1.02	0.48	14.48	11.67	7	0.98	0.00	0.52	0.44	0.08
TRAIN126	4	0.72	4.35	0.43	15.77	9.35	12	0.98	0.01	0.50	0.46	0.08
TRAIN110	5	0.70	2.03	0.53	13.45	9.42	23	0.96	0.02	0.47	0.45	0.09
TRAIN036	11	0.69	5.13	0.40	17.23	12.85	1	1.00	0.03	0.51	0.52	0.05
TRAIN117	13	0.68	1.27	0.47	16.66	14.80	5	0.99	0.04	0.48	0.51	0.08
TRAIN104	14	0.68	5.50	0.47	16.41	11.18	14	0.98	0.03	0.47	0.54	0.06
TRAIN115	16	0.68	3.27	0.39	18.17	15.48	6	0.99	0.05	0.46	0.51	0.06
TRAIN119	19	0.67	7.12	0.35	18.96	11.26	10	0.98	0.01	0.51	0.49	0.07
TRAIN058	20	0.67	8.52	0.33	22.12	19.15	13	0.98	0.05	0.48	0.56	0.04

461

462 **5 Conclusions**

463 In this study we aimed to determine an effective way of tuning the VBS scheme using observations, and also to learn about
 464 the processes controlling OA in Delhi. WRF-Chem model runs with the VBS setup that successfully span the OA
 465 concentrations and O:C ratios from AMS observations can be identified, with many model runs overestimating organic mass
 466 concentrations and underestimating the O:C ratios compared with AMS observations. However, we identified two structural
 467 errors in the model related to a combination of unsuitable diurnal activity cycles applied to the emissions and/or WRF-Chem



468 not being able to capture completely the dynamics of the planetary boundary layer. It is worth mentioning that these structural
469 errors might also be related to representation of other organic aerosol processes not represented by the VBS approach. Recent
470 studies, for example, have examined particle-phase and multiphase chemistry in aqueous aerosols and clouds (Shrivastava et
471 al., 2022), and reactions of SOA precursors with other radicals like chlorine relevant to Indian conditions (Gunthe et al., 2021).

472 The structural errors prevented us from providing an optimised VBS approach in WRF-Chem. However, we were able to apply
473 the emulator in two periods: the full period (1st -29th May) and the 2-4 pm period (14:00- 16:00 hrs, 1st-29th May) to present
474 a methodology to evaluate a model performance using Gaussian emulators and metrics such as FAC2, IOA and MB.
475 Optimization is a stage-by-stage process, future analysis would imply to do an emulation study to address diurnal activity and
476 PBL directly, perhaps using NO_x or total PM.

477 The performance of the two emulators, the full period and the 2-4 pm period, was similar, with the two emulators performing
478 a good prediction of the model outputs and presenting a similar high variance of the anthropogenic SVOC scaling (Parameter
479 5). The model performance would highly improve if we are able to constrain the input values for the parameter 5.

480 When looking at the emulator sensibility analysis, we identified that the parameter anthropogenic SVOC scaling has the highest
481 contribution to the variance, with fractions higher than 70%. This suggests that constraining this parameter would lead to a
482 reduction in the uncertainty in these outputs from the model. Anthropogenic SVOC volatility distribution has little impact on
483 the fraction of variance to O:C ratios with a fraction of variance of around 15%. None of the parameters show a clear variance
484 to improve the model performance.

485 The model evaluation analysis based on FAC2, IOA and MB agreed with the emulator analysis in identifying that using low
486 SVOC volatility distribution and low SVOC scaling would give improved model performance. Based on the MB analysis, for
487 both the full and the 2-4 pm periods, there are runs where the Total OM overprediction was 5 $\mu\text{g}\cdot\text{m}^{-3}$ or lower, i.e, TRAIN110,
488 TRANI121, TRAIN117, etc. This overprediction is considered low compared to the mean Total_OM concentrations of $\sim 20 - 30$
489 $\mu\text{g}\cdot\text{m}^{-3}$. Hence, we are able to identify probable values for the VBS model parameters and are able to model Total OM and
490 O:C ratios in the range of the AMS observations.

491 The combination of the emulator analysis and the model evaluation metrics (FAC2, IOA and mean bias) allowed us to identify
492 the plausible parameter combinations for the analysed periods. The more plausible combinations were found to be with a low
493 SVOC volatility distribution and low SVOC scaling. The methodology presented in this study is shown to be a useful approach
494 to determine the model uncertainty and determine the optimal parameterisation to the WRF-Chem VBS setup. This information
495 is valuable to increase our understanding on secondary organic aerosol formation, which in turn will help to improve regional
496 and global model simulations, emission inventories as well as making informed decisions towards the improvement of air
497 quality in urban environments.

498 **Data availability**

499 Emission generation scripts: https://github.com/douglowe/WRF_UoM_EMIT
500 Scripts for running WRF-Chem (and reducing the outputs to key diagnostics):
501 https://github.com/douglowe/promote_wrfchem_scripts

502 Scenario configuration files, and python script for calculating the “pseudo-age” of the emitted VBS:

503 https://github.com/douglowe/PROMOTE_VBS_scenarios

504 Scenario chemistry input files

505 https://github.com/douglowe/PROMOTE_VBS_scenarios/tree/master/Scenario_Configurations/scenario_chemistry_files_Aug2020

508



509

510 Financial support

511

512 This research has been supported by the UK NERC and MoES, India through the PROMOTE project
513 under the Newton Bhabha Fund programme “Air Pollution and Human Health in a Developing
514 Megacity (APHH-India)”, NERC grant numbers NE/P016480/1 and, NE/P016405. M.S. was supported
515 by the U.S. Department of Energy (DOE) Office of Science, Office of Biological and Environmental
516 Research (BER) through the Early Career Research Program. R.A.Z. acknowledges support from the
517 Office of Science of the U.S. DOE through the Atmospheric System Research (ASR) program at Pacific
518 Northwest National Laboratory (PNNL). PNNL is operated for DOE by Battelle Memorial Institute
519 under contract DE-AC06-76RLO 1830. This paper is based on interpretation of scientific results and in
520 no way reflects the viewpoint of the funding agencies.

521

522 References

- 523 Akherati, A., Cappa, C. D., Kleeman, M. J., Docherty, K. S., Jimenez, J. L., Griffith, S. M., Dusanter, S., Stevens, P.
524 S., and Jathar, S. H.: Simulating secondary organic aerosol in a regional air quality model using the statistical
525 oxidation model – Part 3: Assessing the influence of semi-volatile and intermediate-volatility organic
526 compounds and NO_x, *Atmos. Chem. Phys.*, 19, 4561-4594, 10.5194/acp-19-4561-2019, 2019.
- 527 Archer-Nicholls, S., Lowe, D., Utembe, S., Allan, J., Zaveri, R. A., Fast, J. D., Hodnebrog, Ø., Denier van der Gon,
528 H., and McFiggans, G.: Gaseous chemistry and aerosol mechanism developments for version 3.5.1 of the online
529 regional model, WRF-Chem, *Geosci. Model Dev.*, 7, 2557-2579, 10.5194/gmd-7-2557-2014, 2014.
- 530 Bellouin, N., Baker, L., Hodnebrog, Ø., Olivie, D., Cherian, R., Macintosh, C., Samset, B., Esteve, A., Aamaas, B.,
531 Quaas, J., and Myhre, G.: Regional and seasonal radiative forcing by perturbations to aerosol and ozone
532 precursor emissions, *Atmos. Chem. Phys.*, 16, 13885-13910, 10.5194/acp-16-13885-2016, 2016.
- 533 Bergström, R., Denier van der Gon, H. A. C., Prévôt, A. S. H., Yttri, K. E., and Simpson, D.: Modelling of organic
534 aerosols over Europe (2002-2007) using a volatility basis set (VBS) framework: application of different
535 assumptions regarding the formation of secondary organic aerosol, *Atmos. Chem. Phys.*, 12, 8499-8527,
536 10.5194/acp-12-8499-2012, 2012.
- 537 Bertram, T. H., and Thornton, J. A.: Toward a general parameterization of N₂O₅ reactivity on aqueous particles:
538 the competing effects of particle liquid water, nitrate and chloride, *Atmos. Chem. Phys.*, 9, 8351-8363,
539 10.5194/acp-9-8351-2009, 2009.
- 540 Bran, S. H., and Srivastava, R.: Investigation of PM_{2.5} mass concentration over India using a regional climate
541 model, *Environmental Pollution*, 224, 484-493, <https://doi.org/10.1016/j.envpol.2017.02.030>, 2017.
- 542 Canagaratna, M. R., Jimenez, J. L., Kroll, J. H., Chen, Q., Kessler, S. H., Massoli, P., Hildebrandt Ruiz, L., Fortner,
543 E., Williams, L. R., Wilson, K. R., Surratt, J. D., Donahue, N. M., Jayne, J. T., and Worsnop, D. R.: Elemental ratio
544 measurements of organic compounds using aerosol mass spectrometry: characterization, improved calibration,
545 and implications, *Atmos. Chem. Phys.*, 15, 253-272, 10.5194/acp-15-253-2015, 2015.



546 Carlton, A. G., Bhave, P. V., Napelenok, S. L., Edney, E. O., Sarwar, G., Pinder, R. W., Pouliot, G. A., and Houyoux,
547 M.: Model Representation of Secondary Organic Aerosol in CMAQv4.7, *Environmental Science & Technology*,
548 44, 8553-8560, 10.1021/es100636q, 2010.

549 Carslaw, K. S., Lee, L. A., Regayre, L. A., and Johnson, J. S.: Climate models are uncertain, but we can do
550 something about it, *Eos*, 99, <https://doi.org/10.1029/2018EO093757C>, 2018.

551 Cash, J. M., Langford, B., Di Marco, C., Mullinger, N. J., Allan, J., Reyes-Villegas, E., Joshi, R., Heal, M. R., Acton,
552 W. J. F., Hewitt, C. N., Misztal, P. K., Drysdale, W., Mandal, T. K., Shivani, Gadi, R., Gurjar, B. R., and Nemitz, E.:
553 Seasonal analysis of submicron aerosol in Old Delhi using high-resolution aerosol mass spectrometry: chemical
554 characterisation, source apportionment and new marker identification, *Atmos. Chem. Phys.*, 21, 10133-10158,
555 10.5194/acp-21-10133-2021, 2021.

556 Chen, X., Zhang, Y., Zhao, J., Liu, Y., Shen, C., Wu, L., Wang, X., Fan, Q., Zhou, S., and Hang, J.: Regional modeling
557 of secondary organic aerosol formation over eastern China: The impact of uptake coefficients of dicarbonyls and
558 semivolatile process of primary organic aerosol, *Science of The Total Environment*, 793, 148176,
559 <https://doi.org/10.1016/j.scitotenv.2021.148176>, 2021.

560 Chen, Y., Wild, O., Conibear, L., Ran, L., He, J., Wang, L., and Wang, Y.: Local characteristics of and exposure to
561 fine particulate matter (PM_{2.5}) in four Indian megacities, *Atmospheric Environment: X*, 5, 100052,
562 <https://doi.org/10.1016/j.aeaoa.2019.100052>, 2020a.

563 Chen, Y., Wild, O., Ryan, E., Sahu, S. K., Lowe, D., Archer-Nicholls, S., Wang, Y., McFiggans, G., Ansari, T., Singh,
564 V., Sokhi, R. S., Archibald, A., and Beig, G.: Mitigation of PM_{2.5} and ozone pollution in Delhi: a sensitivity study
565 during the pre-monsoon period, *Atmos. Chem. Phys.*, 20, 499-514, 10.5194/acp-20-499-2020, 2020b.

566 Chutia, L., Ojha, N., Girach, I. A., Sahu, L. K., Alvarado, L. M. A., Burrows, J. P., Pathak, B., and Bhuyan, P. K.:
567 Distribution of volatile organic compounds over Indian subcontinent during winter: WRF-chem simulation
568 versus observations, *Environmental Pollution*, 252, 256-269, <https://doi.org/10.1016/j.envpol.2019.05.097>,
569 2019.

570 Ciarelli, G., Aksoyoglu, S., El Haddad, I., Bruns, E. A., Crippa, M., Poulain, L., Äijälä, M., Carbone, S., Freney, E.,
571 O'Dowd, C., Baltensperger, U., and Prévôt, A. S. H.: Modelling winter organic aerosol at the European scale with
572 CAMx: evaluation and source apportionment with a VBS parameterization based on novel wood burning smog
573 chamber experiments, *Atmos. Chem. Phys.*, 17, 7653-7669, 10.5194/acp-17-7653-2017, 2017.

574 Crooks, M., Connolly, P., and McFiggans, G.: A parameterisation for the co-condensation of semi-volatile
575 organics into multiple aerosol particle modes, *Geosci. Model Dev.*, 11, 3261-3278, 10.5194/gmd-11-3261-2018,
576 2018.

577 Danabasoglu, G., Lamarque, J.-F., Bacmeister, J., Bailey, D. A., DuVivier, A. K., Edwards, J., Emmons, L. K., Fasullo,
578 J., Garcia, R., Gettelman, A., Hannay, C., Holland, M. M., Large, W. G., Lauritzen, P. H., Lawrence, D. M.,
579 Lenaerts, J. T. M., Lindsay, K., Lipscomb, W. H., Mills, M. J., Neale, R., Oleson, K. W., Otto-Bliesner, B., Phillips, A.
580 S., Sacks, W., Tilmes, S., van Kampenhout, L., Vertenstein, M., Bertini, A., Dennis, J., Deser, C., Fischer, C., Fox-
581 Kemper, B., Kay, J. E., Kinnison, D., Kushner, P. J., Larson, V. E., Long, M. C., Mickelson, S., Moore, J. K.,
582 Nienhouse, E., Polvani, L., Rasch, P. J., and Strand, W. G.: The Community Earth System Model Version 2
583 (CESM2), *Journal of Advances in Modeling Earth Systems*, 12, e2019MS001916,
584 <https://doi.org/10.1029/2019MS001916>, 2020.

585 DeCarlo, P. F., Kimmel, J. R., Trimborn, A., Northway, M. J., Jayne, J. T., Aiken, A. C., Gonin, M., Fuhrer, K.,
586 Horvath, T., Docherty, K. S., Worsnop, D. R., and Jimenez, J. L.: Field-deployable, high-resolution, time-of-flight
587 aerosol mass spectrometer, *Anal Chem*, 78, 8281-8289, Doi 10.1021/Ac061249n, 2006.



588 Donahue, N. M., Robinson, A. L., Stanier, C. O., and Pandis, S. N.: Coupled Partitioning, Dilution, and Chemical
589 Aging of Semivolatile Organics, *Environmental Science & Technology*, 40, 2635-2643, 10.1021/es052297c, 2006.
590 Fanourgakis, G. S., Kanakidou, M., Nenes, A., Bauer, S. E., Bergman, T., Carslaw, K. S., Grini, A., Hamilton, D. S.,
591 Johnson, J. S., Karydis, V. A., Kirkevåg, A., Kodros, J. K., Lohmann, U., Luo, G., Makkonen, R., Matsui, H.,
592 Neubauer, D., Pierce, J. R., Schmale, J., Stier, P., Tsigaridis, K., van Noije, T., Wang, H., Watson-Parris, D.,
593 Westervelt, D. M., Yang, Y., Yoshioka, M., Daskalakis, N., Decesari, S., Gysel-Beer, M., Kalivitis, N., Liu, X.,
594 Mahowald, N. M., Myriokefalitakis, S., Schrödner, R., Sfakianaki, M., Tsimpidi, A. P., Wu, M., and Yu, F.:
595 Evaluation of global simulations of aerosol particle and cloud condensation nuclei number, with implications for
596 cloud droplet formation, *Atmos. Chem. Phys.*, 19, 8591-8617, 10.5194/acp-19-8591-2019, 2019.
597 Fast, J. D., Gustafson Jr., W. I., Easter, R. C., Zaveri, R. A., Barnard, J. C., Chapman, E. G., Grell, G. A., and
598 Peckham, S. E.: Evolution of ozone, particulates, and aerosol direct radiative forcing in the vicinity of Houston
599 using a fully coupled meteorology-chemistry-aerosol model, *Journal of Geophysical Research: Atmospheres*,
600 111, <https://doi.org/10.1029/2005JD006721>, 2006.
601 Fountoukis, C., Megaritis, A. G., Skyllakou, K., Charalampidis, P. E., Pilinis, C., Denier van der Gon, H. A. C.,
602 Crippa, M., Canonaco, F., Mohr, C., Prévôt, A. S. H., Allan, J. D., Poulain, L., Petäjä, T., Tiitta, P., Carbone, S.,
603 Kiendler-Scharr, A., Nemitz, E., O'Dowd, C., Swietlicki, E., and Pandis, S. N.: Organic aerosol concentration and
604 composition over Europe: insights from comparison of regional model predictions with aerosol mass
605 spectrometer factor analysis, *Atmos. Chem. Phys.*, 14, 9061-9076, 10.5194/acp-14-9061-2014, 2014.
606 Gadi, R., Shivani, Sharma, S. K., and Mandal, T. K.: Source apportionment and health risk assessment of organic
607 constituents in fine ambient aerosols (PM_{2.5}): A complete year study over National Capital Region of India,
608 *Chemosphere*, 221, 583-596, <https://doi.org/10.1016/j.chemosphere.2019.01.067>, 2019.
609 Grell, G. A., Peckham, S. E., Schmitz, R., McKeen, S. A., Frost, G., Skamarock, W. C., and Eder, B.: Fully coupled
610 "online" chemistry within the WRF model, *Atmos Environ*, 39, 6957-6975,
611 <https://doi.org/10.1016/j.atmosenv.2005.04.027>, 2005.
612 Grieshop, A. P., Logue, J. M., Donahue, N. M., and Robinson, A. L.: Laboratory investigation of photochemical
613 oxidation of organic aerosol from wood fires 1: measurement and simulation of organic aerosol evolution,
614 *Atmos. Chem. Phys.*, 9, 1263-1277, 10.5194/acp-9-1263-2009, 2009.
615 Guenther, A., Karl, T., Harley, P., Wiedinmyer, C., Palmer, P. I., and Geron, C.: Estimates of global terrestrial
616 isoprene emissions using MEGAN (Model of Emissions of Gases and Aerosols from Nature), *Atmos. Chem. Phys.*,
617 6, 3181-3210, 10.5194/acp-6-3181-2006, 2006.
618 Gunthe, S. S., Liu, P., Panda, U., Raj, S. S., Sharma, A., Darbyshire, E., Reyes-Villegas, E., Allan, J., Chen, Y., Wang,
619 X., Song, S., Pöhlker, M. L., Shi, L., Wang, Y., Kommula, S. M., Liu, T., Ravikrishna, R., McFiggans, G., Mickley, L. J.,
620 Martin, S. T., Pöschl, U., Andreae, M. O., and Coe, H.: Enhanced aerosol particle growth sustained by high
621 continental chlorine emission in India, *Nat Geosci*, 14, 77-84, 10.1038/s41561-020-00677-x, 2021.
622 Hersbach, H., Bell, B., Berrisford, P., Biavati, G., Horányi, A., Muñoz Sabater, J., Nicolas, J., Peubey, C., Radu, R.,
623 Rozum, I., Schepers, D., Simmons, A., Soci, C., Dee, D., and Thépaut, J.-N.: ERA5 hourly data on pressure levels
624 from 1979 to present. Copernicus Climate Change Service (C3S) Climate Data Store (CDS). Copernicus,
625 10.24381/cds.bd0915c6, 2018.
626 Huang, L., Zhu, Y., Zhai, H., Xue, S., Zhu, T., Shao, Y., Liu, Z., Emery, C., Yarwood, G., Wang, Y., Fu, J., Zhang, K.,
627 and Li, L.: Recommendations on benchmarks for numerical air quality model applications in China – Part 1:
628 PM_{2.5} and chemical species, *Atmos. Chem. Phys.*, 21, 2725-2743, 10.5194/acp-21-2725-2021, 2021.
629 World Air Quality: <https://www.iqair.com/>, access: 05/08/2021, 2021.



- 630 Jain, S., Sharma, S. K., Vijayan, N., and Mandal, T. K.: Seasonal characteristics of aerosols (PM_{2.5} and PM₁₀) and
631 their source apportionment using PMF: A four year study over Delhi, India, *Environmental Pollution*, 262,
632 114337, <https://doi.org/10.1016/j.envpol.2020.114337>, 2020.
- 633 Jat, R., Gurjar, B. R., and Lowe, D.: Regional pollution loading in winter months over India using high resolution
634 WRF-Chem simulation, *Atmos Res*, 249, 105326, <https://doi.org/10.1016/j.atmosres.2020.105326>, 2021.
- 635 Johnson, J. S., Regayre, L. A., Yoshioka, M., Pringle, K. J., Lee, L. A., Sexton, D. M. H., Rostron, J. W., Booth, B. B.
636 B., and Carslaw, K. S.: The importance of comprehensive parameter sampling and multiple observations for
637 robust constraint of aerosol radiative forcing, *Atmos. Chem. Phys.*, 18, 13031-13053, 10.5194/acp-18-13031-
638 2018, 2018.
- 639 Johnson, J. S., Regayre, L. A., Yoshioka, M., Pringle, K. J., Turnock, S. T., Browse, J., Sexton, D. M. H., Rostron, J.
640 W., Schutgens, N. A. J., Partridge, D. G., Liu, D., Allan, J. D., Coe, H., Ding, A., Cohen, D. D., Atanacio, A., Vakkari,
641 V., Asmi, E., and Carslaw, K. S.: Robust observational constraint of uncertain aerosol processes and emissions in
642 a climate model and the effect on aerosol radiative forcing, *Atmos. Chem. Phys.*, 20, 9491-9524, 10.5194/acp-
643 20-9491-2020, 2020.
- 644 Kanakidou, M., Seinfeld, J. H., Pandis, S. N., Barnes, I., Dentener, F. J., Facchini, M. C., Van Dingenen, R., Ervens,
645 B., Nenes, A., Nielsen, C. J., Swietlicki, E., Putaud, J. P., Balkanski, Y., Fuzzi, S., Horth, J., Moortgat, G. K.,
646 Winterhalter, R., Myhre, C. E. L., Tsigaridis, K., Vignati, E., Stephanou, E. G., and Wilson, J.: Organic aerosol and
647 global climate modelling: a review, *Atmos. Chem. Phys.*, 5, 1053-1123, 10.5194/acp-5-1053-2005, 2005.
- 648 Kompalli, S. K., Suresh Babu, S. N., Satheesh, S. K., Krishna Moorthy, K., Das, T., Boopathy, R., Liu, D., Darbyshire,
649 E., Allan, J. D., Brooks, J., Flynn, M. J., and Coe, H.: Seasonal contrast in size distributions and mixing state of
650 black carbon and its association with PM_{1.0} chemical composition from the eastern coast of India, *Atmos.*
651 *Chem. Phys.*, 20, 3965-3985, 10.5194/acp-20-3965-2020, 2020.
- 652 Lane, T. E., Donahue, N. M., and Pandis, S. N.: Simulating secondary organic aerosol formation using the
653 volatility basis-set approach in a chemical transport model, *Atmos Environ*, 42, 7439-7451,
654 <https://doi.org/10.1016/j.atmosenv.2008.06.026>, 2008.
- 655 Lee, H.-J., Jo, H.-Y., Song, C.-K., Jo, Y.-J., Park, S.-Y., and Kim, C.-H.: Sensitivity of Simulated PM_{2.5} Concentrations
656 over Northeast Asia to Different Secondary Organic Aerosol Modules during the KORUS-AQ Campaign,
657 *Atmosphere*, 11, 1004, 2020.
- 658 Lee, L. A., Carslaw, K. S., Pringle, K. J., Mann, G. W., and Spracklen, D. V.: Emulation of a complex global aerosol
659 model to quantify sensitivity to uncertain parameters, *Atmos. Chem. Phys.*, 11, 12253-12273, 10.5194/acp-11-
660 12253-2011, 2011.
- 661 Li, J.-L., Zhang, M.-G., Gao, Y., and Chen, L.: Model analysis of secondary organic aerosol over China with a
662 regional air quality modeling system (RAMS-CMAQ), *Atmospheric and Oceanic Science Letters*, 9, 443-450,
663 10.1080/16742834.2016.1233798, 2016.
- 664 May, A. A., Levin, E. J. T., Hennigan, C. J., Riipinen, I., Lee, T., Collett Jr., J. L., Jimenez, J. L., Kreidenweis, S. M.,
665 and Robinson, A. L.: Gas-particle partitioning of primary organic aerosol emissions: 3. Biomass burning, *Journal*
666 *of Geophysical Research: Atmospheres*, 118, 11,327-311,338, <https://doi.org/10.1002/jgrd.50828>, 2013.
- 667 Olivier, J., Peters, J., Granier, C., Pétron, G., Muller, J. F., and Wallens, S.: POET inventory - Metadata, GEIA-
668 ACCENT emission data portal, France, 2003.
- 669 Reyes-Villegas, E., Green, D. C., Priestman, M., Canonaco, F., Coe, H., Prévôt, A. S. H., and Allan, J. D.: Organic
670 aerosol source apportionment in London 2013 with ME-2: exploring the solution space with annual and
671 seasonal analysis, *Atmos. Chem. Phys.*, 16, 15545-15559, 10.5194/acp-16-15545-2016, 2016.



- 672 Reyes-Villegas, E., Panda, U., Darbyshire, E., Cash, J. M., Joshi, R., Langford, B., Di Marco, C. F., Mullinger, N. J.,
673 Alam, M. S., Crilley, L. R., Rooney, D. J., Acton, W. J. F., Drysdale, W., Nemitz, E., Flynn, M., Voliotis, A.,
674 McFiggans, G., Coe, H., Lee, J., Hewitt, C. N., Heal, M. R., Gunthe, S. S., Mandal, T. K., Gurjar, B. R., Shivani, Gadi,
675 R., Singh, S., Soni, V., and Allan, J. D.: PM1 composition and source apportionment at two sites in Delhi, India,
676 across multiple seasons, *Atmos. Chem. Phys.*, 21, 11655-11667, 10.5194/acp-21-11655-2021, 2021.
- 677 Robinson, A. L., Donahue, N. M., Shrivastava, M. K., Weitkamp, E. A., Sage, A. M., Grieshop, A. P., Lane, T. E.,
678 Pierce, J. R., and Pandis, S. N.: Rethinking Organic Aerosols: Semivolatile Emissions and Photochemical Aging,
679 *Science*, 315, 1259-1262, doi:10.1126/science.1133061, 2007.
- 680 Shivani, Gadi, R., Sharma, S. K., and Mandal, T. K.: Seasonal variation, source apportionment and source
681 attributed health risk of fine carbonaceous aerosols over National Capital Region, India, *Chemosphere*, 237,
682 124500, <https://doi.org/10.1016/j.chemosphere.2019.124500>, 2019.
- 683 Shrivastava, M., Fast, J., Easter, R., Gustafson Jr, W. I., Zaveri, R. A., Jimenez, J. L., Saide, P., and Hodzic, A.:
684 Modeling organic aerosols in a megacity: comparison of simple and complex representations of the volatility
685 basis set approach, *Atmos. Chem. Phys.*, 11, 6639-6662, 10.5194/acp-11-6639-2011, 2011.
- 686 Shrivastava, M., Berg, L. K., Fast, J. D., Easter, R. C., Laskin, A., Chapman, E. G., Gustafson Jr., W. I., Liu, Y., and
687 Berkowitz, C. M.: Modeling aerosols and their interactions with shallow cumuli during the 2007 CHAPS field
688 study, *Journal of Geophysical Research: Atmospheres*, 118, 1343-1360, <https://doi.org/10.1029/2012JD018218>,
689 2013.
- 690 Shrivastava, M., Andreae, M. O., Artaxo, P., Barbosa, H. M. J., Berg, L. K., Brito, J., Ching, J., Easter, R. C., Fan, J.,
691 Fast, J. D., Feng, Z., Fuentes, J. D., Glasius, M., Goldstein, A. H., Alves, E. G., Gomes, H., Gu, D., Guenther, A.,
692 Jathar, S. H., Kim, S., Liu, Y., Lou, S., Martin, S. T., McNeill, V. F., Medeiros, A., de Sá, S. S., Shilling, J. E.,
693 Springston, S. R., Souza, R. A. F., Thornton, J. A., Isaacman-VanWertz, G., Yee, L. D., Ynoue, R., Zaveri, R. A.,
694 Zelenyuk, A., and Zhao, C.: Urban pollution greatly enhances formation of natural aerosols over the Amazon
695 rainforest, *Nature Communications*, 10, 1046, 10.1038/s41467-019-08909-4, 2019.
- 696 Shrivastava, M., Rasool, Q. Z., Zhao, B., Octaviani, M., Zaveri, R. A., Zelenyuk, A., Gaudet, B., Liu, Y., Shilling, J. E.,
697 Schneider, J., Schulz, C., Zöger, M., Martin, S. T., Ye, J., Guenther, A., Souza, R. F., Wendisch, M., and Pöschl, U.:
698 Tight Coupling of Surface and In-Plant Biochemistry and Convection Governs Key Fine Particulate Components
699 over the Amazon Rainforest, *ACS Earth and Space Chemistry*, 6, 380-390, 10.1021/acsearthspacechem.1c00356,
700 2022.
- 701 Shrivastava, M. K., Lane, T. E., Donahue, N. M., Pandis, S. N., and Robinson, A. L.: Effects of gas particle
702 partitioning and aging of primary emissions on urban and regional organic aerosol concentrations, *Journal of*
703 *Geophysical Research: Atmospheres*, 113, <https://doi.org/10.1029/2007JD009735>, 2008.
- 704 Stewart, G. J., Nelson, B. S., Acton, W. J. F., Vaughan, A. R., Farren, N. J., Hopkins, J. R., Ward, M. W., Swift, S. J.,
705 Arya, R., Mondal, A., Jangirh, R., Ahlawat, S., Yadav, L., Sharma, S. K., Yunus, S. S. M., Hewitt, C. N., Nemitz, E.,
706 Mullinger, N., Gadi, R., Sahu, L. K., Tripathi, N., Rickard, A. R., Lee, J. D., Mandal, T. K., and Hamilton, J. F.:
707 Emissions of intermediate-volatility and semi-volatile organic compounds from domestic fuels used in Delhi,
708 India, *Atmos. Chem. Phys.*, 21, 2407-2426, 10.5194/acp-21-2407-2021, 2021a.
- 709 Stewart, G. J., Nelson, B. S., Acton, W. J. F., Vaughan, A. R., Hopkins, J. R., Yunus, S. S. M., Hewitt, C. N., Nemitz,
710 E., Mandal, T. K., Gadi, R., Sahu, L. K., Rickard, A. R., Lee, J. D., and Hamilton, J. F.: Comprehensive organic
711 emission profiles, secondary organic aerosol production potential, and OH reactivity of domestic fuel
712 combustion in Delhi, India, *Environmental Science: Atmospheres*, 1, 104-117, 10.1039/D0EA00009D, 2021b.
- 713 Tilmes, S., Hodzic, A., Emmons, L. K., Mills, M. J., Gettelman, A., Kinnison, D. E., Park, M., Lamarque, J.-F., Vitt, F.,
714 Shrivastava, M., Campuzano-Jost, P., Jimenez, J. L., and Liu, X.: Climate Forcing and Trends of Organic Aerosols



715 in the Community Earth System Model (CESM2), *Journal of Advances in Modeling Earth Systems*, 11, 4323-4351,
716 <https://doi.org/10.1029/2019MS001827>, 2019.

717 Topping, D., Connolly, P., and McFiggans, G.: Cloud droplet number enhanced by co-condensation of organic
718 vapours, *Nat Geosci*, 6, 443-446, 10.1038/ngeo1809, 2013.

719 Tsigaridis, K., Daskalakis, N., Kanakidou, M., Adams, P. J., Artaxo, P., Bahadur, R., Balkanski, Y., Bauer, S. E.,
720 Bellouin, N., Benedetti, A., Bergman, T., Bernsten, T. K., Beukes, J. P., Bian, H., Carslaw, K. S., Chin, M., Curci, G.,
721 Diehl, T., Easter, R. C., Ghan, S. J., Gong, S. L., Hodzic, A., Hoyle, C. R., Iversen, T., Jathar, S., Jimenez, J. L., Kaiser,
722 J. W., Kirkevåg, A., Koch, D., Kokkola, H., Lee, Y. H., Lin, G., Liu, X., Luo, G., Ma, X., Mann, G. W., Mihalopoulos,
723 N., Morcrette, J. J., Müller, J. F., Myhre, G., Myriokefalitakis, S., Ng, N. L., O'Donnell, D., Penner, J. E., Pozzoli, L.,
724 Pringle, K. J., Russell, L. M., Schulz, M., Sciare, J., Seland, Ø., Shindell, D. T., Sillman, S., Skeie, R. B., Spracklen, D.,
725 Stavrakou, T., Steenrod, S. D., Takemura, T., Tiitta, P., Tilmes, S., Tost, H., van Noije, T., van Zyl, P. G., von Salzen,
726 K., Yu, F., Wang, Z., Wang, Z., Zaveri, R. A., Zhang, H., Zhang, K., Zhang, Q., and Zhang, X.: The AeroCom
727 evaluation and intercomparison of organic aerosol in global models, *Atmos. Chem. Phys.*, 14, 10845-10895,
728 10.5194/acp-14-10845-2014, 2014.

729 Tsimpidi, A. P., Karydis, V. A., Zavala, M., Lei, W., Molina, L., Ulbrich, I. M., Jimenez, J. L., and Pandis, S. N.:
730 Evaluation of the volatility basis-set approach for the simulation of organic aerosol formation in the Mexico City
731 metropolitan area, *Atmos. Chem. Phys.*, 10, 525-546, 10.5194/acp-10-525-2010, 2010.

732 Tsimpidi, A. P., Karydis, V. A., Pandis, S. N., and Lelieveld, J.: Global combustion sources of organic aerosols:
733 model comparison with 84 AMS factor-analysis data sets, *Atmos. Chem. Phys.*, 16, 8939-8962, 10.5194/acp-16-
734 8939-2016, 2016.

735 von Schneidmesser, E., Monks, P. S., Allan, J. D., Bruhwiler, L., Forster, P., Fowler, D., Lauer, A., Morgan, W. T.,
736 Paasonen, P., Righi, M., Sindelarova, K., and Sutton, M. A.: Chemistry and the Linkages between Air Quality and
737 Climate Change, *Chemical Reviews*, 115, 3856-3897, 10.1021/acs.chemrev.5b00089, 2015.

738 Watson, L. A., Shallcross, D. E., Utembe, S. R., and Jenkin, M. E.: A Common Representative Intermediates (CRI)
739 mechanism for VOC degradation. Part 2: Gas phase mechanism reduction, *Atmos Environ*, 42, 7196-7204,
740 <https://doi.org/10.1016/j.atmosenv.2008.07.034>, 2008.

741 Wiedinmyer, C., Akagi, S. K., Yokelson, R. J., Emmons, L. K., Al-Saadi, J. A., Orlando, J. J., and Soja, A. J.: The Fire
742 INventory from NCAR (FINN): a high resolution global model to estimate the emissions from open burning,
743 *Geosci. Model Dev.*, 4, 625-641, 10.5194/gmd-4-625-2011, 2011.

744 Wild, O., Voulgarakis, A., O'Connor, F., Lamarque, J. F., Ryan, E. M., and Lee, L.: Global sensitivity analysis of
745 chemistry-climate model budgets of tropospheric ozone and OH: exploring model diversity, *Atmos. Chem.*
746 *Phys.*, 20, 4047-4058, 10.5194/acp-20-4047-2020, 2020.

747 Willmott, C. J., Robeson, S. M., and Matsuura, K.: A refined index of model performance, *International Journal*
748 *of Climatology*, 32, 2088-2094, <https://doi.org/10.1002/joc.2419>, 2012.

749 Zaveri, R. A., Easter, R. C., Fast, J. D., and Peters, L. K.: Model for Simulating Aerosol Interactions and Chemistry
750 (MOSAIC), *Journal of Geophysical Research: Atmospheres*, 113, <https://doi.org/10.1029/2007JD008782>, 2008.

751 Zhang, Q., Jimenez, J. L., Canagaratna, M. R., Allan, J. D., Coe, H., Ulbrich, I., Alfarra, M. R., Takami, A.,
752 Middlebrook, A. M., Sun, Y. L., Dzepina, K., Dunlea, E., Docherty, K., DeCarlo, P. F., Salcedo, D., Onasch, T., Jayne,
753 J. T., Miyoshi, T., Shimojo, A., Hatakeyama, S., Takegawa, N., Kondo, Y., Schneider, J., Drewnick, F., Borrmann,
754 S., Weimer, S., Demerjian, K., Williams, P., Bower, K., Bahreini, R., Cottrell, L., Griffin, R. J., Rautiainen, J., Sun, J.
755 Y., Zhang, Y. M., and Worsnop, D. R.: Ubiquity and dominance of oxygenated species in organic aerosols in
756 anthropogenically-influenced Northern Hemisphere midlatitudes, *Geophys Res Lett*, 34, L13801, Artn L13801

<https://doi.org/10.5194/acp-2022-463>
Preprint. Discussion started: 12 July 2022
© Author(s) 2022. CC BY 4.0 License.



757 Doi 10.1029/2007gl029979, 2007.

758